Mismatch repair and homologous recombination are yin-yang partners in hybrid zygote meiosis

Chi-Ning Chuang[1,*], Ya-Ling Hung[1,*], Hong-Xiang Kim[1,2,*], Jhong-Syuan Yao[1], Hou-Cheng Liu[1], Sheng-Yuan Chen[1], Lavernchy Jovanska[1], Yi-Ping Hsueh[1,2], Ruey-Shyang Chen[2], and Ting-Fang Wang[1,2,#]

[1]Institute of Molecular Biology, Academia Sinica, Taipei, 11529, Taiwan

[2]Department of Biochemical Science and Technology, National Chiayi University, Taiwan

[*]These authors contributed equally to this work

[#]Corresponding author. Email: tfwang@gate.sinica.edu.tw

Keywords:

Meiosis; Hybrid infertility; Homologous recombination; Mismatch repair; Meiosis; DSB repair

In brief

Excessive interhomolog recombination leads to hybrid infertility

Highlights

- Homologous recombination (HR) antagonizes mismatch repair (MMR) in hybrid meiosis.
- Anti-MMR mutations of HR genes (*RAD51*, *RAD54,* or *ZMM*) cause hybrid sterility.
- Hybrid sterility is due to excessive (rather than insufficient) interhomolog HR.
- Hybrid sterility-inducing anti-MMR mutations can be rescued by repressing MMR genes.

Authors' email addresses:

Chi-Ning Chuang	chining@gate.sinica.edu.tw
Ya-Ling Hung	yaling121216@gmail.com
Hong-Xiang Kim	hongxiangj76@gmail.com
Jhong-Syuan Yao	shinglay840529@gmail.com
Sheng-Yuan Chen	sychen98@gate.sinica.edu.tw
Hou-Chen Liu	hc666@gate.sinica.edu.tw
Lavernchy Jovanska	lavernchy@yahoo.com
Yi-Ping Hsueh	yph@gate.sinica.edu.tw
Ruey-Shyang Chen	rschen@mail.ncyu.edu.tw
Ting-Fang Wang	tfwang@gate.sinica.edu.tw

SUMMARY (<150 words)

Mismatch repair (MMR) is believed to prevent homologous recombination (HR) between homologous chromosomes, causing infertility in hybrids between closely related species. We report that HR and MMR are yin-yang partners in the response to genetic polymorphisms and that several budding yeast HR genes (i.e., *RAD51*, *RAD54*, *ZMM*) exhibit anti-MMR activities. This yin-yang relationship biases MMR in wild-type interspecies (*Saccharomyces cerevisiae*/*Saccharomyces paradoxus*) hybrid zygotes and intraspecies *S. cerevisiae* hybrid zygotes with anti-MMR mutations, resulting in excessive (rather than insufficient) interhomolog HR, including negative crossover interference, allelic conversion or even disruption. The anti-MMR function of *S. cerevisiae* Rad54 prevails over its accessory role in promoting Rad51-mediated strand exchange during hybrid meiosis. Srs2 (the yeast ortholog of *Esherichia coli* UvrD helicase) facilitates the MMR system by dissembling Rad51-ssDNA presynaptic filaments. Sgs1 (the yeast ortholog of *E. coli* RecQ helicase) acts after MMR-dependent recognition of heteroduplex mismatches to promote crossover clustering and allelic switching.

INTRODUCTION

Meiosis, a specialized cell division of sexual eukaryotes, generates haploid gametes from diploid precursor cells. This process occurs via one round of DNA replication and two sequential cell divisions, i.e., meiosis I (MI) and meiosis II (MII). After replication, each homologous chromosome generates two sister chromatids that are paired and held together via the cohesion complexes. The sister chromatid pairs then interact and form a bivalent that encompasses a total of four copies of double-stranded DNA (dsDNA). In most species, this process requires the formation of chiasmata via homologous recombination (HR) to physically connect the homologous chromosomes. HR is initiated via programmed induction of DNA double-strand breaks (DSBs) between premeiotic S phase and meiotic prophase I. In the budding yeast *Saccharomyces cerevisiae* (the subject of this study), DSBs are first resected 5′ to 3′ to form ~1 kilobase (kb) of single-stranded DNA (ssDNA) overhangs, which are protected by replication protein A (RPA). Two RecA-like recombinases (ubiquitous Rad51 and meiosis-specific Dmc1) cooperate to repair DSBs preferentially via the interhomolog (IH) HR pathway, i.e., using a homologous non-sister chromosome rather than a sister chromatid as a template. This process involves invasion of an intact template and formation of a displacement loop (D-loop), followed by DNA repair synthesis of the free 3' end in the D-loop. Rad51 and Dmc1 do not act alone. Rad51 has several accessory factors, such as the PCSS complex (Psy3•Csm2•Shu1•Shu2), Rad52, Rad54, the Rad55•Rad57 heterodimer, Rad59, Srs2, Pif1 and Hed1. Dmc1's accessory factors include Rad51, Tid1 (also called Rdh54), the Mei5•Sae3 heterodimer, and the Hop2•Mnd1 heterodimer (1). The Psy3•Csm2 complex is structurally similar to the Rad51 dimer and can stabilize the Rad51-ssDNA nucleoprotein filaments (2). Rad52 exerts dual roles. First, it associates with RPA and functions with the Rad55•Rad57 heterocomplex to assemble Rad51-ssDNA nucleoprotein filaments (3).

Rad59 regulates associations of Rad52 with DNA DSBs (4). Second, the strand annealing activity of Rad52 promotes second-end capture in DSB repair to form stabilized joint molecules, ultimately leading to the generation of Holliday junctions (5,6). The Rad51 patches on ssDNA can stimulate filament assembly of Dmc1 *in vitro* (7). Srs2 is a member of the superfamily 1 (Sf1a) helicases that move in the 3′ → 5′ direction relative to the bound strand of nucleic acid (8,9). Srs2 binds to Rad51 (not Dmc1), competitively ejects Rad52 and the Rad55•Rad57 complex, and then disassembles the Rad51-ssDNA presynaptic filament (10-13). Unlike Rad52, the PCSS complex does not appear to promote Rad51 function during meiosis by antagonizing Srs2 (13). Dmc1 is a potent inhibitor of Srs2 (14). Rad54 and Tid1 are members of the Swi2/Snf2 family of dsDNA-dependent ATPases that preferentially facilitate the homology pairing and strand exchange activities of Rad51 and Dmc1, respectively (15). Rad54 binds tightly to Rad51-ssDNA and acts downstream of Srs2 to promote Rad51-mediated homolog pairing and strand exchange reactions (16). Hed1 is a meiosis-specific inhibitor of Rad51 (17) that prevents Rad51 from interacting with Rad54 (18). It has been postulated that meiotic recombination occurs in two temporally distinct phases (19). During Phase 1, Rad51 is inhibited by Hed1, and Dmc1 mediates the IH-HR that promotes homolog synapsis. In Phase 2, Rad51 becomes active and functions with Rad54 to repair residual DSBs, making increasing use of sister chromatids. The transition from Phase 1 to Phase 2 is controlled by a meiotic recombination checkpoint through the action of a meiosis-specific effector kinase, Mek1. Pif1, an ATP-dependent 5′-to-3′ DNA helicase, specifically promotes Rad51-mediated IH-HR, but not Dmc1-mediated IH-HR (19). Ultimately, the IH-HR pathway produces two recombination products: crossovers (COs) and non-crossovers (NCOs; also called gene conversions). IH-COs are the primary source of genetic diversity in gametes, whereas IH-NCOs involve the unidirectional transfer of genetic information. Some IH-COs result in chiasmata

and, together with sister chromatid cohesion, allow spindle tension to be generated when homologous chromosomes begin to segregate during MI (see review in (1)).

DSB repair in both NCOs and COs involves synthesis-dependent strand annealing (SDSA), often with multiple rounds of strand invasion. In *S. cerevisiae*, IH-NCOs form earlier than IH-COs and are mainly produced via the SDSA pathway. IH-NCO formation is abolished during early meiosis in *S. cerevisiae* mutants lacking Sgs1 (the yeast homolog of *E. coli* and mammalian RecQ helicases) (20). CO-specific double Holliday junction formation occurs via processes involving branch migration as an integral feature, which can be separated from repair of the break itself (21). If homologs harbor different alleles, the resulting hybrid DNA (heteroduplex) by homologous recombination will contain mismatches. The mismatches present in the heteroduplex are detected genetically as departures from Mendelian segregation (4^+:4^-, based on the eight ssDNA strands present) in haploid meiotic products. Heteroduplex mismatches on only one homolog (asymmetric heteroduplex) produce 5^+:3^- or 3^+:5^- marker segregation (half conversion), as well as 6^+:2^- or 2^+:6^- marker segregation (full conversion). Allelic gene conversion or switching occurs during meiosis between heterozygotic sites, resulting in heteroduplex mismatches that are then recognized and/or corrected by the mismatch repair (MMR) system (see below), thus causing one of the alleles to be converted to the other. This process can cause non-Mendelian segregation (NMS), i.e., 3^+:1^-, 1^+:3^-, 4^+:0^-, or 0^+:4^- alleles in tetrads (based on the four dsDNA duplexes present). In contrast, Mendelian segregation (MS) results in 2^+:2^- tetrads (22-26).

Most proteins involved in the prokaryotic and eukaryotic MMR systems are conserved both structurally and functionally. During the MMR process in *E. coli*, heteroduplex mismatches are first recognized by the MutS homodimer. Subsequently, a ternary complex comprising DNA, MutS, and MutL is formed in a reaction requiring ATP. A nick is then introduced by MutH into

the unmethylated DNA strand at a hemimethylated d(GATC) site. Next, the ATP-bound MutL dimer loads the UrvD helicase onto the nicked DNA. The UvrD loading event ensures that the helicase is loaded onto the correct strand to translocate in the 3′ to 5′ direction toward the mismatch (27). Mismatch recognition in most studied eukaryotes is trigged by two evolutionarily conserved MutS complexes, i.e., Msh2•Msh3 (MutSα) and Msh2•Msh6 (MutSβ). MutSβ is primarily involved in repairing base-base and small insertion/deletion loop mismatches, whereas MutSα acts primarily on insertion/deletion loop mismatches up to 12 nucleotides in length (28). During mismatch correction, the MutLα (Mlh1•Pms1) endonuclease is then activated in a mismatch-dependent manner by MutSβ (or MutSα), RPA, PCNA, RFC, and DNA polymerase δ in reconstituted 3′-nick-directed MMR reactions (29). MutLα functions as the primary factor in repairing heteroduplex mismatches (30). MutLβ (Mlh1•Mlh2) is a non-essential accessory factor that acts to enhance the activity of MutLα during vegetative growth (31). Using a yeast strain with an HO endonuclease-induced DSB that can be repaired by single-strand annealing (SSA) between flanking homologous sequences, heteroduplex rejection was found to be mediated by Sgs1 and Msh2, but not by the yeast MutL proteins. Moreover, correction of heteroduplex mismatches within the SSA intermediates required MutLα to the same extent as Msh2 (32). During meiosis, MutLβ forms a dynamic ensemble with a meiosis-specific DNA helicase Mer3 at the Dmc1-dependent D-loops to limit Sgs1-dependent NCO *in vivo* (33,34). MutLγ is a Msh2-stimulated endonuclease that mediates CO-specific resolution of double Holliday junctions (33,35-40). UvrD can dismantle *E. coli* RecA nucleoprotein filaments in *E. coli* (41). The primary function of Srs2, the yeast paralog of UvrD, is to dissemble the Rad51-ssDNA presynaptic filament during HR (42). It remains unclear if Srs2 is also involved in yeast MMR or nucleotide excision repair.

Two mechanisms have been reported to regulate chromosome-wide IH-CO positions (43-46). First, the "CO assurance rule" reflects the fact that each pair of homologous chromosomes must receive at least one obligatory chiasma during the diplotene stage of meiosis prophase I because a chiasma ensures proper chromosome segregation at MI. Second, IH-COs too close to each other might result in diminished sister chromatin cohesion and tension at MI. The "CO interference rule" reflects the fact that superfluous IH-COs lead to chromosome nondisjunction (NDJ) and aneuploidy. In classical genetics, interference (γ) is defined as 1 – (coefficient of coincidence; c.o.c.), where c.o.c is calculated by dividing the actual double recombinant frequency by the expected double recombinant frequency. Within many sexual eukaryotes, including *S. cerevisiae*, two subclasses of IH-COs co-exist. The class I IH-CO pathway accounts for 70-85% of COs in *S. cerevisiae* and requires a group of meiosis-specific ZMM proteins, including Zip1, the Zip2•Zip4•Spo16 (ZZS) complex, Mer3 DNA helicase, the Msh4•Msh5 (MutSγ) complex and MutLγ (33,35-40,47). This group of IH-CO products is interference-sensitive or interfering, with formation of COs in relative proximity to each other appearing to be suppressed (24,48). The ZMM group of proteins also controls assembly of the synaptonemal complex (SC), representing a protein lattice that connects paired homologous chromosomes in meiotic prophase (47). It has been reported previously that CO assurance requires all ZMM proteins and a full-length SC. In contrast, CO interference requires the normal assembly of recombination complexes containing MutSγ, but it does not require ZZS- or Zip3-dependent extension of the SC (49). Class II IH-COs were classically believed to be non-interfering in several sexual eukaryotes (44,48,50). However, a recent study has indicated that they might be interfering in *S. cerevisiae* (51). This pathway is independent of ZMM proteins and MutLγ, but involves the Mms4•Mus81 endonuclease complex (48) and, to a lesser degree, Yen1/GEN1 resolvase (Holliday junction 5' flap endonuclease) and

the Slx1•Slx4 endonuclease heterocomplex (52,53). Srs2 was reported previously to promote Mms4-mediated resolution of D-loops (54-57), yet it has been shown using a Srs2 separation-of-function mutant that the ability of Srs2 to remove Rad51 from ssDNA is its primary role during HR (42). Mms4•Mus81 might collaborate with Sgs1 to promote joint molecule resolution *in vivo* and to direct meiotic recombination toward IH interactions that promote proper chromosome segregation (58,59). In sexual eukaryotes (e.g., the fission yeast *Schizosaccharomyces pombe* and the free-living ciliate *Tetrahymena thermophila*) that lost the SC during their evolution, Sgs1 and the Mms4•Mus81 complex are sufficient to execute meiotic recombination (58-60). Not only does Sgs1 prevent aberrant crossing-over by suppressing formation of multichromatid joint molecules, but it also functions as an IH-CO-promoting factor (20,26,38,61-65).

Meiosis is highly related to speciation. Hybrid zygotes between closely related species are often sterile or inviable. Hybrid infertility is an important feature of the speciation process, acting as a reproductive isolating barrier. For almost 30 years, it was believed that the two haploid genome sequences in hybrid zygotes are too diverged to cross over efficiently during meiosis, resulting in MI NDJ and aneuploidy. The MMR system was thought to be the major impediment to HR during meiosis in sexual eukaryotes and interspecific sexual conjugation in prokaryotes, as the requirement for DNA sequence homology during sexual reproduction is relaxed in mutants deficient in anti-recombination genes (25,66-80). Mismatch recognition triggers heteroduplex correction and/or rejection, whereby helicases disassemble recombination intermediates that contain heteroduplexes. The heteroduplex mismatches are recognized and corrected by the MMR system via removal and resynthesis of strands over large regions. Deleting *MSH2* inactivates both heteroduplex rejection and MMR, thereby preserving heteroduplex patterns and allowing inference of parental strand contributions from genotypes of spores in tetrads (66,67,69-74,81). It has also

been reported that Sgs1 acts downstream of Msh2-mediated mismatch recognition to unwind nascent recombination intermediates containing a high density of heteroduplex base pair mismatches (80). Accordingly, the fertility of interspecies *Saccharomyces cerevisiae* W303/*Saccharomyces paradoxus* N17 hybrid zygotes can be increased to the level of non-hybrids by introducing the P_{CLB2}-*MSH2* and P_{CLB2}-*SGS1* constructs. The genomic sequences of *S. cerevisiae* and *S. paradoxus* differ by >12% (82). P_{CLB2} is the native promoter of the mitosis-specific B-type cyclin gene *CLB2* that is deactivated during meiosis (83), thereby specifically repressing *MSH2* and *SGS1* during that cell division (82). Given that Sgs1 seems to possess conflicting functions during meiosis, it is not entirely clear how the MMR system and Sgs1 constitute an absolute barrier to DSB repair in interspecies hybrid zygotes. First, Sgs1 promotes the SDSA pathway to generate NCOs and COs via multiple rounds of strand invasion (20,26). Second, Sgs1 acts downstream of the MMR system to unwind nascent recombination intermediates (80). Third, Sgs1 and Srs2 have opposing effects on the regulation of homeologous recombination (i.e., HR between partially homologous sequences). Suppression of recombination between homeologous sequences was found to be enhanced in *srs2* mutants but reduced in *sgs1* mutants (84). Further investigations are needed to reveal the functional relationships between the MMR system, Sgs1 and Srs2.

Most of our current knowledge about *S. cerevisiae* meiotic recombination was mainly derived from studies of purebred diploid strains (e.g., SK1/SK1, BR/BR or S288c/S288c) and intraspecies hybrid diploid strains (e.g., SK1/S288c, SK1/BR or S288c/BR) because they are fertile and produce many viable spores (80,81). The nucleotide sequences (or genotypes) of two haploid genomes in purebred zygotes are nearly identical to each other due to long-term inbreeding, whereas those in intraspecies hybrid zygotes often possess a significant degree of sequence

heterogeneity. For example, the genomic sequences of *S. cerevisiae* SK1 and S288c haploid strains differ by ~2%, including 212,640 base pairs (~1.76%) of single nucleotide polymorphisms (SNPs) and 944,944 base pairs (~7.83%) of insertions and deletions (InDels)(85). Notably, genome-wide mapping of meiotic recombination products (in tetrads with four viable spores) revealed that deletion of *MSH2* from the SK1/S288c hybrid zygotes only reduced COs by ~20% (81).

In this report, we propose that HR and MMR are yin-yang balanced partners during meiosis of SK1/S288c hybrid zygotes, and that HR proteins can antagonize the MMR system in those zygotes. This yin-yang relationship is biased in purebred zygotes (e.g., SK1/SK1) towards HR and in interspecies *S. cerevisiae*/*S. paradoxus* hybrid zygotes toward MMR. Accordingly, HR proteins with anti-MMR activity exhibit two distinct properties. First, they are preferentially required for fertility (i.e., the formation of viable spores) of SK1/S288c hybrid zygotes compared to SK1/SK1 purebred zygotes. Second, the low fertility (spore viability) phenotype of SK1/S288c hybrid zygotes with anti-MMR mutation(s) can be rescued (at least partly) by removal or meiotic repression of MMR genes (e.g., *MSH2*). We have uncovered several anti-MMR genes that regulate the yin-yang relationship between HR and MMR in hybrid meiosis.

RESULTS

Identification of anti-MMR genes preferentially required for intraspecies hybrid meiosis rather than for purebred meiosis

We used three different wild-type *S. cerevisiae* diploid strains for genetic screening of anti-MMR genes. The SK1/SK1-*HL* purebred strains carry a well-characterized DSB and meiotic recombination hotspot, i.e., *HIS4::LEU2*-(*NBamHI*)*/his4-X::LEU2*-(*NgoMIV*)-*URA3* (referred to

herein as "*HL*") (Figure 1A) (23,24,86). *HL* constitutes a recombination reporter in which DSBs form at high frequency within a narrow zone of ~150 base pairs (bp), making this hotspot suited for genetic analysis, as well as for physical analyses of DSB resection and the subsequent choice of DSB repair via the IH-HR or inter-sister (IS-HR) pathways (23,87,88). We applied polymerase chain reaction (PCR) to amplify a DNA fragment containing the *HIS4::LEU2*-(*New BamHI*) allele from the SK1 haploid strain and then integrated it into a haploid S288c strain. The resulting SK1/S288c-*HL** hybrid diploid cells carry the same HL DSB hotspot, except that a point mutation (*) was introduced to mutate the *XhoI* restriction site adjacent to probe A (Figure 1B). To investigate the impacts of longer and denser heteroduplex mismatches during DSB repair, we also generated a SK1/S288c-*HL**-*SNP+* hybrid strain that carries the *HIS4::LEU2*-(*New BamHI*)-*SNP+/his4-X::LEU2*-(*NgoMIV*)-*URA3* hotspot. Compared to the *HIS4::LEU2*-(*New BamHI)* allele, the *HIS4::LEU2*-(*New BamHI*)-*SNP+* allele possesses 180 exogenously introduced single nucleotide polymorphisms (SNPs), as it was modified to harbor single nucleotide sequence changes every 29 ± 9 bp for 1,633 bp to the left of the DSB site and 944 bp to the right (Figure 1B). A similar approach was used previously to study repeated strand invasion and extensive branch migration in *S. cervisiae* meiosis (26). Southern hybridization revealed that all three of these diploid strains are feasible for quantification of IH-CO and IH-NCO recombination products (Figure 1C-1F; see below).

Next, we screened >50 different mutants (Supplemental Information, Table S1) known to be involved in DSB repair and/or MMR in *S. cerevisiae* meiosis. In brief, all diploid cells were incubated at 30 °C in sporulation medium for at least 24 hours and then scored for their capability to form mature tetrads and viable sexual spores. Spore viability was determined by isolating the four single spores from each tetrad on YPDA plates. Their genotypes and fertility phenotypes (i.e.,

ability to form tetrads and/or viable spores) are provided in Supplemental Information Dataset 1 (DS1) and DS2, respectively. First, we confirmed that *rad54*Δ (89) and *dmc*1Δ *hed*1Δ (90) resulted in fewer viable spores in two hybrid zygotes (i.e., SK1/S288c-*HL** and SK1/S288c-*HL**-*SNP*+) compared to a purebred zygote (i.e., SK1/SK1-*HL*). As reported previously (91), *rad51-II3A* hardly affected meiotic recombination or spore viability of the SK1/SK1-*HL* purebred zygotes (Figure 2A). The Rad51-II3A mutant has a normal DNA binding site I and a defective DNA binding site II. Therefore, it can assemble onto ssDNA and form nucleoprotein filaments, but it is defective in capturing a homologous dsDNA template for homology pairing and strand exchange (91).

Nearly all single mutants we examined (e.g., *rad51-II3A*, *rad51*Δ*N* and *rad51*Δ; Figure 2A) exhibited similar meiotic phenotypes in generating tetrads and viable spores in the SK1/S288c-*HL** and SK1/S288c-*HL**-*SNP*+ hybrid zygotes (DS2). Rad51-ΔN is a hypomorphic mutant lacking the N-terminal domain (NTD, 1-66 amino acid residues). Removal of the NTD from Rad51 reduces by >95% its steady-state protein levels but retains most of its DSB repair activities during vegetative growth and meiosis (92).

These mutants were classified into five distinct groups based on their ability to form tetrads and viable spores in the wild-type SK1/SK1-*HL** purebred zygotes, as well as in both wild-type and P_{CLB2}-*MSH2* SK1/S288c-*HL**-*SNP*+ hybrid zygotes, respectively.

The group I mutants include *rad51*Δ, *rad52*Δ, *dmc1*Δ, and *tid1*Δ. Dmc1, Tid1, Rad51, and Rad52 are indispensable for homology-directed DSB repair in both purebred and hybrid meiosis (1). Both purebred and hybrid zygotes hosting these mutants formed no or very few tetrads and/or viable spores and were insensitive to the introduction of P_{CLB2}-*MSH2* (Figures 2B and DS2).

The group II mutants (P_{CLB2}-*SGS1*, *sgs1*Δ-*C795* and *sgs1*Δ) produced similar numbers of viable spores in the SK1/SK1-*HL** purebred zygotes (66.7±6.1%, 73.6±6.1%, and 44.0±4.2%) and in the SK1/S288c-*HL**-*SNP+* hybrid zygotes (73.1±2.1%, 66.2±4.2%, and 53.2±4.2%), respectively (Figure 2B and DS2). *sgs1*Δ-C795, in which the carboxy-terminal 795 amino acids have been removed, was shown previously to be a separation-of-function mutant that defines the Sgs1 function important for meiosis (61). Sgs1 does not meet the criteria for an anti-MMR protein in our assay, as introduction of P_{CLB2}-*MSH2* into the P_{CLB2}-*SGS1* SK1/S288c-*HL**-*SNP+* hybrid zygotes slightly reduced the spore viability from 73.1±2.1% to 54.4±8.6% (Figure 2B).

The group III mutants (P_{CLB2}-*MPH1*, P_{CLB2}-*MMS4* and P_{CLB2}-*PIF1*) produced more viable spores in the SK1/SK1-*HL** purebred zygotes (95.4±1.6%, 72.2±2.8%, and 94.4±1.4%) than the SK1/S288c-*HL**-*SNP+* hybrid zygotes (54.6±9.9%, 29.2±6.4%, and 56.9±14.6%) and the P_{CLB2}-*MSH2* SK1/S288c-HL*-SNP+ hybrid zygotes (29.2±8.4%, 20.8±7.3%, and 53.1±9.6%) (Figures 2B and DS2). Mph1 is the *S. cerevisiae* ortholog of the mammalian Fanconi anemia complementation group M (FANCM) helicase that prevents precocious DSB strand exchange between sister chromatids before homologs have completed pairing, thereby ensuring high levels of IH-COs and IH-NCOs between non-sister homologous chromosomes (21). Therefore, Mph1, Mms4, and Pif1 do not meet the criteria for anti-MMR proteins. *ku70*Δ also belongs to this group. Ku70 and Ku80 form a heterodimeric Ku complex in a wide range of eukaryotes that exerts multiple roles, including in DSB repair via the nonhomologous end joining (NHEJ) pathway and telomere maintenance (28,93). The values of spore viability we determined are: *ku70*Δ SK1/SK1-*HL** (93.5±5.6%); *msh2*Δ SK1/SK1-*HL** (83.3±7.2%); *ku70*Δ *msh2*Δ SK1/SK1-*HL** (79.6±0.8%); *ku70*Δ SK1/S288c-*HL**-*SNP+* (60.6±11.2%); *msh2*Δ SK1/S288c-*HL**-*SNP+* (75.0±3.7%); and *ku70*Δ *msh2*Δ SK1/S288c-*HL**-*SNP+* (50.9±5.3%) (Figure 2B and DS2).

The group IV mutants are "anti-MMR" mutants, which we divided into two subgroups (IV-A and IV-B) according to the degree of hybrid infertility. Except for *mer3*Δ, all other "IV-A" mutants showed more pronounced fertility (spore viability) defects in the SK1/S288c-*HL**-*SNP*+ hybrid zygotes than in the SK1/SK1-*HL** purebred zygotes, including *dmc1*Δ *hed1*Δ, *rad54*Δ, *rad51-II3A*, *rad51*-Δ*N*, *rad51-A320V*, *rad51-Y388H*, *rad51-G393D*, *rad59*Δ, P_{CLB2}-*SRS2*, *mer3*Δ, *zip1*Δ, and *zip4*Δ (Figures 2C-2D). Mer3 is indispensable for both purebred and hybrid meiosis, as both *mer3*Δ purebred and hybrid zygotes hardly formed tetrads. The low spore viability defects of all group IV-A mutants (including *mer3*Δ) in the SK1/S288c-*HL**-*SNP*+ hybrid zygotes could be rescued (at least in part) by introducing P_{CLB2}-*MSH2*. Mer3 is a meiosis-specific DNA helicase having several functions. It can stimulate 3′-to-5′ heteroduplex extension of Rad51, thereby stabilizing nascent joint molecules via DNA heteroduplex extension to permit capture of the second processed end of a dsDNA break, a step required for the formation of IH-CO products (94). Mer3 also physically interacts with Dmc1 to antagonize the anti-recombinase activities of Sgs1 (34), and thus selectively affects IH-CO but not IH-NCO formation. Moreover, Mer3 competes with the Pif1 5′-to-3′ DNA helicase for binding to the PCNA clamp loader RFC, thereby limiting polymerase delta (Pol δ)-mediated DNA synthesis during DSB repair (95). Pif1 specifically promotes Rad51-mediated IH-HR but not Dmc1-meditated IH-HR (19). The anti-MMR activity of Mer3 might be related to the finding that the Mer3•MutLβ complex preferentially recognizes D-loops because purified Mer3 and MutLβ both preferentially recognize these structures, providing a mechanism for limiting gene conversion *in vivo* (33). The Rad51-A320V, Rad51-Y388H, and Rad51-G393D mutant proteins are defective in binding to Rad52 and/or Srs2, yet retain the ability (equivalent to wild-type) to interact with Rad54, Tid1, and Rad59 (96). Rad59 interacts with Rad52 and augments Rad52's activity in the SSA pathway (97). Srs2 may facilitate

the MMR system by antagonizing Rad51 because its primary role during HR is to remove Rad51 from ssDNA (42). Zip1 is the main structural component of the SC central element (98) and antagonizes Mph1-mediated dissociation of late occurring joint molecules (21). The Zip2•Zip4(Spo22)•Spo16 (ZZS) complex performs multiple distinct activities. Zip4 acts as a hub for physical interactions with components of the chromosome axis (e.g., Red1 and Hop1), with components of the SC central element (e.g., Ecm11), and with the crossover machinery (99,100).

The "IV-B" mutants exhibited much weaker or no anti-MMR activities, including *zip2-ΔXPF*, *zip4-N919Q*, *ecm11Δ*, *rad51-NTD3A*, and *msh4Δ* (Figures 2E). The Zip4-N919Q point mutant specifically abolishes the Zip4-Ecm11 interaction, leading to loss of Ecm11 binding to chromosomes and defective SC assembly (100). Spo16 binds the C-terminal XPF domain of Zip2 to form a meiosis-specific complex that shares structural similarities to the structure-specific XPF–ERCC1 nuclease, although it lacks endonuclease activity. The Zip2-ΔXPF mutant protein lacks the XPF domain, which mediates the non-catalytic DNA recognition function of the Zip2•Spo16 complex that promotes IH-CO formation via binding to joint molecule recombination intermediates. Despite a minor difference between CO levels, both the sporulation efficiency and spore viability of the *zip2-ΔXPF* mutant are significantly higher than those of the *zip2Δ* mutant (88,101). Therefore, the anti-MMR activity of the ZZS complex is significantly affected by loss of the Zip4-Ecm11 interaction (100) or the Zip2-Spo16 interaction (88,101). Rad51-NTD3A is a phosphorylation-defective mutant in which the three serine residues of the SQ motifs (S2Q, S12Q, and S30Q) of Rad51 are mutated into alanines. All three SQ motifs of wild-type Rad51 are phosphorylated by two DNA damage checkpoint kinases ($Mec1^{ATR}$ and $Tel1^{ATM}$) during meiosis. We have reported previously that the maximum steady-state levels of Rad51-NTD3A in meiotic cells is ~30% those of wild-type Rad51, but the *rad51-NTD3A* mutant generated as many (>90%)

viable spores as wild-type cells (92). Msh4 and Msh5 form a meiosis-specific MutSγ heterodimer that is not involved in recognizing heteroduplex mismatches or MMR, but it does facilitate crossing over by binding and stabilizing nascent recombination intermediates (88,102-104). The *msh4*Δ SK1/SK1 purebred hybrid zygotes generated ~80% viable spores, whereas both *msh4*Δ and *msh4*Δ P_{CLB2}-*MSH2* SK1/S288c-*HL*-SNP+* hybrid zygotes only generated ~30% and ~40% viable spores, respectively.

The only group V mutant is *zip3*Δ, which resulted in more viable spores in the *MSH2* SK1/S288c-*HL*-SNP+* hybrid zygotes (~50%) than in *MSH2* SK1/SK1-*HL* purebred zygotes (~30%) and P_{CLB2}-*MSH2* SK1/S288c-*HL*-SNP+* hybrid zygotes (~35%) (Figure 2D). *S. cerevisiae* Zip3 and its paralogs RNF212 and HEI10 in other sexual eukaryotes are E3 ligases of ubiquitin and/or small ubiquitin-like modifier (SUMO) (105-109). Zip3 and MutLγ are enriched at class I COs, appearing as bright foci on pachytene chromosomes (45,105,108-110).

Lastly, we confirmed that the genetic results obtained from the SK1/SK1-*HL* purebred zygotes and the SK1/S288c-*HL*-SNP+* hybrid zygotes are consistent with those obtained from SK1(*a, VIII, rgC*)/SK1(*α, VIII, RGc*) and S288c(*a, VIII, rgC*)/SK1(*α, VIII, RGc*) zygotes with three spore-autonomous fluorescent maker genes (*RFP, GFP*, and *CFP*) (111) (Table 1 and DS2), where *MATa, MATα*, chromosome VIII, *CEN8::RFP, CEN8*, *ARG4::GFP*, *ARG4, THR1::CFP* and *THR1* are indicated as *a*, *α*, *VIII, R*, *r*, *G*, *g, C*, and *c,* respectively.

These genetic results reveal several intriguing and important features of the anti-MMR proteins. First, the anti-MMR function of Rad51 requires a sufficient amount of catalytically active Rad51 (i.e., *rad51-ΔN* and *rad51-NTD3A*) (92), Rad51's binding capability to Rad52 and/or Srs2 (i.e., *rad51-A320V*, *rad51-Y388H*, and *rad51-G393D*) (96), the homology pairing and strand exchange activities of Rad51 itself (i.e., *rad51-II3A*) (91), and Rad51's homology pairing and

strand exchange cofactor Rad54 (i.e., *rad54*Δ) (89,112,113). Second, the group of ZMM proteins responds differentially to genetic polymorphism and MMR in hybrid zygotes. Mer3, like Dmc1 and Tid1, is indispensable for sporulation and the formation of viable spores. The anti-MMR activities of Mer3, Zip1 and the ZZS complex are significantly stronger than that of the MutSγ complex. In contrast, Zip3 may function independently or in weak coordination with the MMR system in hybrid zygotes.

Rad51 and Dmc1 utilize different mechanisms to encounter heteroduplex mismatches and the MMR system during homology-directed DSB repair

Controversy exists regarding the roles of Rad51 and Dmc1 in tolerating heteroduplex mismatches during the homology pairing and strand exchange reactions. First, *S. cerevisiae,* Rad51 and Dmc1 exhibit similar mismatch tolerability during homology pairing strand exchange *in vivo* (114). Second, Dmc1 is superior to Rad51 in tolerating heteroduplex mismatches in budding yeast, fission yeast, and mammals (85,90,115-120). Two hypothetical cryogenic electron microscopy (cryo-EM) protein models have been used to propose that two critical amino acids in eukaryotic Rad51 (i.e., *H. sapiens* Val273 and Asp274, *S. cerevisiae* Val311 and Asp332) and Dmc1 (*H. sapiens* Pro274 and Gly27, *S. cerevisiae* Pro267 and Gly268) might explain why Dmc1 exhibits higher mismatch tolerability than Rad51 (119,120) (Table S1 and DS2). Our genetic results do not support this hypothesis because the capability of wild-type Rad51 in generating viable spores in both SK1/SK1 *dmc1*Δ *hed1*Δ purebred zygotes and SK1/S288c hybrid *dmc1*Δ *hed1*Δ zygotes was similar to that of Rad51-V331P, Rad51-D332G or the Rad51-V331P D322G double mutant. Moreover, Pro267 is dispensable for Dmc1's function in meiosis because both *dmc1-P267V* purebred and hybrid zygotes (96.8±0.8% and 84.3±1.6%) produced as many viable spores as purebred and hybrid wild-

type zygotes (96.4±5.9% and 85.1±3.9%). In contrast, Gly268 is essential for Dmc1's catalytic function. Like *dmc1*Δ, both *dmc1-G268D* and the *dmc1-P267V dmc1-G268D* double mutant elicited severe meiotic arrest before MI and resulted in no tetrads being generated in SK1/SK1 purebred and SK1/S288c hybrid zygotes (DS2).

We postulate that Rad51 and Dmc1 might utilize different mechanisms to tolerate heteroduplex mismatches and antagonize the MMR system, respectively. Since Dmc1 and Tid1 (Rdh54) do not possess anti-MMR activities (this study) and Dmc1 can tolerate heteroduplex mismatches (85,90,115-120), the Dmc1-mediated IH-HR pathway likely adopts two different approaches to tolerate or antagonize heteroduplex mismatches. Before heteroduplex mismatches are recognized by the Msh2-containing MMR complexes (i.e., Phase I of early prophase (19)), the Dmc1-ssDNA nucleoprotein filaments can tolerate heteroduplex mismatches during the homology pairing and strand exchange reactions, thereby initiating IH-HR and promoting homolog synapsis (19). This early function of Dmc1 requires Tid1 (15), Rad51, Rad52, Rad51's ability for ssDNA binding, and Dmc1's (but not Rad51's) capability to capture dsDNA during the homology pairing and strand exchange reactions (91). Accordingly, *dmc1*Δ*, tid1*Δ, *rad51*Δ, and *rad52*Δ all result in strong infertility defects in both SK1/SK1 purebred zygotes and SK1/S288c hybrid zygotes. Introduction of P_{CLB2}-*MSH2* into the SK1/S288c-*HL*-SNP+* hybrid zygotes also cannot rescue the infertility defects of the *dmc1*Δ*, tid1*Δ, *rad51*Δ, and *rad52*Δ mutants (Figure 2A-2B and DS2).

Dmc1 mediates the IH-HR that promotes ZMM-mediated homolog synapsis during meiotic Phase 1 (19). Based on our genetic results (Figure 2C-2E and DS2), we suggest that Mer3, Zip1, the ZZS complex, and MutSγ may sequentially and/or collectively facilitate Dmc1-mediated IH-HR after heteroduplex mismatches are recognized by the Msh2-containing MMR complexes. This hypothesis is consistent with the findings of several previous reports. First, Mer3 can

stimulate DNA heteroduplex extension (94). Second, Mer3 directly interacts with Dmc1 and competes with Pif1 and Sgs1 (34,95). Pif1 specifically promotes Rad51-mediated IH-HR but not Dmc1-meditated IH-HR (19). Third, Mer3 recruits MutLβ to facilitate D-loop recognition and limits Sgs1-mediated gene conversion *in vivo* (33).

The anti-MMR activity of Rad51 preferentially targets MutSα, MutSβ, and MutLα rather than MutLβ or MutLγ

Next, we observed that, in the SK1/S288c-*HL**-*SNP+* hybrid zygotes, the spore viability was P_{CLB2}-*MSH6* (84.7±2.8%), P_{CLB2}-*MSH3* (82.4±7.9%), *msh2*Δ (75.0.±3.7%), *mlh2*Δ (72.2±6.1%), P_{CLB2}-*MSH6 rad51-II3A* (70.8±8.4%), P_{CLB2}-*MSH2* (70.3±10.1%), *mlh3*Δ (63.4±1.6%), *pms1*Δ (62.0±4.0%), *pms1*Δ *rad51-II3A* (57.6±4.6%), P_{CLB2}-*MSH3 rad51-II3A* (56.5±7.0%), *msh2*Δ *rad51-II3A* (49.4±4.0%), P_{CLB2}-*MSH2 rad51-II3A* (41.1±12.1%), *mlh2*Δ *rad51-II3A* (29.2±1.4%), *rad51-II3A* (21.9±6.9%), and *mlh3*Δ *rad51-II3A* (0.9±0.8%) (Figure 2F and DS2). As reported previously (82), P_{CLB2} indeed effectively repressed meiotic expression of *MSH2*, *MSH3* and *MSH6*. We then confirmed by immunoblotting experiments using anti-HA antibodies that P_{CLB2} can diminish the steady-state proteins levels of HA-tagged Msh2, Sgs1, and Srs2 in sporulating cells but not in vegetative cells, respectively (Figure S1). We conclude that the anti-MMR activity of Rad51 can act on MutS-driven mismatch recognition and MutLα-mediated mismatch correction, but not MutLγ-dependent IH-CO, in the SK1/S288c-*HL**-*SNP+* hybrid zygotes.

Genetic requirements of the anti-MMR functions of Rad51 and Rad54 in hybrid meiosis

Like P_{CLB2}-*MSH2,* P_{CLB2}-*SRS2* and P_{CLB2}-*SGS1* slightly increased hybrid fertility (spore viability) of *rad51-II3A* SK1/S288c-*HL**-*SNP+* hybrid zygotes. Unlike P_{CLB2}-*MSH2,* P_{CLB2}-*SRS2* did not

increase hybrid fertility (spore viability) of *rad54*Δ SK1/S288c-*HL**-*SNP+* hybrid zygotes. P_{CLB2}-*MPH1*, P_{CLB2}-*PIF1* and P_{CLB2}-*MMS4* further decreased the hybrid fertility of *rad51-II3A* SK1/S288c-*HL**-*SNP+* hybrid zygotes. The respective order of spore viability is: P_{CLB2}-*SRS2 rad51-II3A* (48.6±6.4%) ~ P_{CLB2}-*MSH2 rad54*Δ (48.6±15.5%) > P_{CLB2}-*MSH2 rad51-II3A* (41.1±12.1%) > P_{CLB2}-*SGS1 rad51-II3A* (34.7±3.7%) > *rad51-II3A* (21.9±6.9%) > P_{CLB2}-*MPH1 rad51-II3A* (15.3±9.7%) > P_{CLB2}-*MMS4 rad51-II3A* (6.9±2.4%) ~ P_{CLB2}-*SRS2 rad54*Δ (6.5±5.3%) > P_{CLB2}-*PIF1 rad54*Δ (3.7±4.0%) ~ P_{CLB2}-*MMS4 rad54*Δ (2.8±1.4%) ~ *rad54*Δ (0.9±0.8%) ~ P_{CLB2}-*MPH1 rad54*Δ (0.5±0.8%) > P_{CLB2}-*PIF1 rad51-II3A* (no tetrads) (Figure 2C-2G and DS2).

$DiBAC_4(5)$ [Bis-(1,3-dibutylbarbituric acid) pentamethine oxonol] (121) and DAPI (4, 6-diamidino-2-phenylindole) staining experiments (122,123) further revealed that >80% wild-type SK1/S288c-*HL**-*SNP+* hybrid zygotes sporulated (Figure S2A) and completed MI (Figure S2B). *rad51-II3A, rad54*Δ, P_{CLB2}-*SRS2,* P_{CLB2}-*SRS2 rad51-II3A* and *rad54*Δ SK1/S288c-*HL**-*SNP+* hybrid zygotes slightly affected sporulation (Figure S2A), as ~80% wild-type and only 30-60% mutant SK1/S288c-*HL**-*SNP+* hybrid zygotes completed MI, respectively, 9 hours after being transferred into sporulation medium (Figure S2B).

Both wild-type and *rad51-II3A* SK1/S288c-*HL**-*SNP+* hybrid zygotes with *mer3*Δ, *zip1*Δ, or *zip4*Δ hardly sporulated (Figure S3A), completed MI (Figure S3B), or generated mature tetrads (Figure 2G). The *zip3*Δ *rad51-II3A* SK1/S288c-*HL**-*SNP+* hybrid zygotes also hardly form mature tetrads, whereas the *msh4*Δ *rad51-II3A* SK1/S288c-*HL**-*SNP+* hybrid zygotes form 2.8±2.8% viable spores (Figure 2G. In contrast, ~60% of the *mms4*Δ and *mms4*Δ *rad51-II3A* hybrid zygotes sporulated (Figure S3A) and completed MI (Figure S3B). These results support our conclusion that ZMM proteins (Mer3, Zip1 and the ZZS complex) but not the Mms4•Mus81 endonuclease complex possess anti-MMR activities.

We also confirmed that the genetic results obtained from the SK1/SK1-*HL* purebred zygotes and the SK1/S288c-*HL*-SNP+* hybrid zygotes are consistent with those obtained from SK1(*a, VIII, rgC*)/SK1(*α, VIII, RGc*) purebred zygotes and S288c(*a, VIII, rgC*)/SK1(*α, VIII, RGc*) hybrid yeast zygotes (Table 1 and DS2).

Yeast Srs2, like *E. coli* UvrD, facilitates the MMR system

UvrD can dismantle RecA nucleoprotein filaments during the process of nucleotide excision repair (NER) and methyl-directed MMR (41), whereas the main function of Srs2 in HR is to dissemble the Rad51-ssDNA nucleoprotein filaments (16). Accordingly, Srs2 and UvrD not only are highly conserved in their amino acid sequences and protein structures, but also utilize similar anti-HR activities to facilitate the MMR system in *E. coli* and *S. cerevisiae*, respectively. We observed that, like P_{CLB2}-*MSH2,* P_{CLB2}-*SRS2* could rescue (at least in part) the low fertility defects of SK1/S288c-*HL*-SNP+* hybrid zygotes with the Rad51-II3A*,* Rad51-A320V, Rad51-Y388H, and Rad51-G393D mutations, respectively. The spore viability of the corresponding single and double mutants is: *rad51-G393D* (15.7±2.1%); *rad51-II3A* (21.9±6.9%); *rad51-A320V* (28.7±9.5%); *rad51-Y388H* (31.5±7.9%); *rad51-II3A* P_{CLB2}-*MSH2* (41.1±12.1%); *rad51-A320V* P_{CLB2}-*SRS2* (47.2±14.1%); *rad51-II3A* P_{CLB2}-*SRS2* (48.6±6.4%); *rad51-Y388H* P_{CLB2}-*SRS2* (52.2±3.2%); *rad51-G393D* P_{CLB2}-*MSH2* (53.7±18.9%); *rad51-G393D* P_{CLB2}-*SRS2* (55.2±2.1%); *rad51-Y388H* P_{CLB2}-*MSH2* (62.0±8.5%); and *rad51-A320V* P_{CLB2}-*MSH2* (65.3±4.2%) (Figure 2C). Rad51-A320V, Rad51-Y338H and Rad51-G393D are impaired in terms of Rad52 binding and/or the Srs2 interaction, but they are proficient in interacting with Rad54, Tid1, and Rad59 (96). Thus, our results indicate that yeast Srs2, like *E. coli* UvrD, belongs to the MMR system.

Rad54 acts downstream of Srs2 during homeologous recombination

Unlike P_{CLB2}-*MSH2,* P_{CLB2}-*SRS2* failed to rescue the low fertility phenotype of both *rad54*Δ and *dmc1*Δ *hed1*Δ hybrid zygotes, including both SK1/S288c-*HL**-*SNP*+ (Figure 2C) and S288c(*a,rgC*)/SK1(*α,RGc*) (DS2). The order of spore viability in the SK1/S288c-*HL**-*SNP*+ hybrid zygotes is: *rad54*Δ (0.9±0.8%) ~ *dmc1*Δ *hed1*Δ P_{CLB2}-*SRS2* (0.9±0.8%) < *rad54*Δ P_{CLB2}-*SRS2* (6.5±5.3%) < *dmc1*Δ *hed1*Δ (19.4±7.3%) < *dmc1*Δ *hed1*Δ P_{CLB2}-*MSH2* (48.1±4.9%) ~ *rad54*Δ P_{CLB2}-*MSH2* (48.6±15.5%) (Figure 2C and DS2). These results are consistent with the findings of two previous reports. First, Rad54 binds tightly to Rad51-ssDNA and acts downstream of Srs2 (16). Second, in the *dmc1*Δ *hed1*Δ hybrid zygotes, Rad51 activity is negatively regulated by Mek1-mediated Rad54 phosphorylation, which prevents Rad54 from interacting with Rad51 (124).

Since both *rad54*Δ and *dmc1*Δ *hed1*Δ purebred zygotes produced more viable spores than either *rad54*Δ or *dmc1*Δ *hed1*Δ hybrid zygotes (Figure 2 and DS2), Rad54 exerts dual roles in hybrid zygotes, i.e., it promotes Rad51-mediated HR and it antagonizes the MMR system. When more heteroduplex mismatches are generated in hybrid zygotes, the anti-MMR function of Rad54 prevails over its pro-HR function.

Sgs1 acts after the MMR system during homeologous recombination

We found that the P_{CLB2}-*SGS1* SK1/SK1-*HL* purebred zygotes (66.7±6.1%) and the P_{CLB2}-*SGS1* SK1/S288c-*HL**-*SNP*+ hybrid zygotes (73.1±2.1%) produced similar amounts of viable spores. In contrast, the P_{CLB2}-*SRS2* SK1/S288c-*HL**-*SNP*+ hybrid zygotes (32.4±8.4%) produced fewer viable spores than the P_{CLB2}-*SRS2* SK1/SK1-*HL* purebred zygotes (59.7±11.4%) (Figure 2B and DS2). P_{CLB2}-*MSH2* had the opposite effect to P_{CLB2}-*SRS2* and P_{CLB2}-*SGS1* in the SK1/S288c-*HL**-

SNP+ hybrid zygotes, with the order of spore viability being P_{CLB2}-*SRS2* (32.4±8.4%) < P_{CLB2}-*MSH2* P_{CLB2}-*SRS2* (44.3±3.9%) < P_{CLB2}-*MSH2* P_{CLB2}-*SGS1* (54.4±8.6%) < P_{CLB2}-*MSH2* (70.3±10.1%) ~ P_{CLB2}-*SGS1* (73.1±2.1%) (Figure 2B and DS2). P_{CLB2}-*SRS2* proved slightly better than P_{CLB2}-*SGS1* in rescuing the low fertility phenotype of *rad51-II3A* SK1/S288c-*HL*-SNP+* hybrid zygotes, with the order of spore viability being *rad51-II3A* (21.9±6.9%) < *rad51-II3A* P_{CLB2}-*SGS1* (34.7±3.7%) ~ *rad51-II3A* P_{CLB2}-*MSH2* (41.1±12.1%) < *rad51-II3A* P_{CLB2}-*SRS2* (48.6±6.4%) (Figure 2C and DS2). These results are consistent with three previous reports showing that *SRS2* and *SGS1* respond differentially to heteroduplex mismatches and the MMR system in SK1/S288c hybrid zygotes. First, suppression of recombination between homeologous sequences was found to be enhanced in *srs2* mutants but reduced in *sgs1* mutants (84). Second, the primary function of Srs2 in HR is to remove Rad51 from ssDNA (42). Third, Sgs1 acts downstream of mismatch recognition by the Msh2-containing MMR complex in hybrid meiosis (80). Consequently, we conclude that Srs2 and Sgs1 facilitate the MMR system respectively before and after mismatch recognition by the Msh2-containing MMR complex.

ZMM-dependent class I IH-CO products are (normally) produced in *rad51-II3A* hybrid zygotes

To determine if the low fertility phenotype of the *rad51-II3A* hybrid zygotes is due to insufficient IH-CO products, we performed physical analyses to quantify both IH-CO and IH-NCO products generated at the *HL* hotspot in the SK1/SK1-*HL* purebred zygotes, as well as those at the HL^* hotspot and the HL^*-*SNP+* hotspot in the SK1/S288c hybrid zygotes, respectively. Genomic DNA was isolated 24 hours after the corresponding diploid zygotes were transferred into sporulation medium, digested by *XhoI* and *NgoMIV*, visualized by Southern hybridization with "probe A", and

then quantified with a TyphoonFLA 9000 biomolecular imager (125). A point mutation was introduced in *HL** to mutate the *XhoI* restriction site adjacent to "probe A". The IH-CO* fragments in both SK1/S288c-*HL** and SK1/S288c-*HL**-*SNP*+ hybrid zygotes (~5.7 kb) were longer than the IH-CO* fragment in the SK1/SK1-*HL* purebred zygotes (~4.6 kb). The length of the IH-NCO* DNA fragments (~4.3 kb) was the same in all zygotes (Figure 1A and 1B).

The quantities of both IH-CO* and IH-NCO* products in the SK1/SK1-*HL* purebred zygotes were not affected by *rad51-II3A, rad54*Δ, or *rad51-G393D*, but they were significantly reduced by *dmc1*Δ *hed1*Δ (Figure 1C, lanes 1-5; Figure 1E, left panels). These results are consistent with those of two previous studies on *rad51-II3A* (91) and *dmc1*Δ *hed1*Δ (90). Our $DiBAC_4(5)$ and DAPI staining experiments also revealed that *dmc1*Δ *hed1*Δ had more profound impacts on (Figure S2A) and MI (Figure S2C-S2D) than *rad51-II3A*, *rad54*Δ or *rad51-G393D* in both SK1/SK1-*HL* purebred and SK1/S288c-*HL**-*SNP*+ hybrid zygotes, respectively.

Compared to the SK1/SK1-*HL* purebred zygotes, the increase in genome-wide sequence polymorphism displayed by SK1/S288c-*HL** hybrid zygotes had a more profound impact on IH-NCO* than IH-CO* at this DSB hotspot. The numbers of IH-CO* in wild-type (*RAD51*) and *rad51-II3A* SK1/SK1-*HL* purebred zygotes (Figure 1C, lanes 1-2; Figure 2E, upper left panel) were similar to those exhibited by wild-type and *rad51-II3A* SK1/S288c-*HL** hybrid zygotes (Figure 1C, lanes 6-7; Figure 1E, upper middle panel). In contrast, the quantities of IH-NCO* in *RAD51* and *rad51-II3A* SK1/SK1-*HL* purebred zygotes (Figure 1C, lanes 1-2; Figure 1E, lower left panel) were significantly lower than those in wild-type and *rad51-II3A* SK1/S288c-*HL** hybrid zygotes (Figure 1C, lanes 6-7; Figure 1E, lower middle panel).

The numbers of both IH-CO* and IH-NCO* in wild-type and *rad51-II3A* SK1/S288c-*HL**-*SNP*+ hybrid zygotes (Figure 1C, lanes 8-9; Figure 1E, middle panels) were lower than those

presented by both wild-type and *rad51-II3A* SK1/S288c-*HL** hybrid zygotes (Figure 1C, lanes 6-7; Figure 2E, middle panels). Thus, the introduction of 180 exogenous SNPs into the *HL** hotspot significantly reduced both IH-CO* and IH-NCO* products at this DSB hotspot. Notably, the quantities of IH-CO* and IH-NCO* at this DSB hotspot (Figure 1E and 1F) cannot explicitly explain the low fertility defects of *rad51-II3A* SK1/S288c- *HL** and *rad51-II3A* SK1/S288c-*HL**-*SNP+* hybrid zygotes (Figure 2 and DS2). The same conclusion is applicable to another four anti-MMR mutations of the SK1/S288c-*HL*-SNP+* hybrid zygotes, i.e., *rad51-II3A, rad54*Δ, *rad51-G393D,* and *dmc1*Δ *hed1*Δ (Figure 1C, lanes 9-12; Figure 1E, right panels). Introduction of P_{CLB2}-*MSH2* into wild-type and those four anti-MMR mutants did not significantly alter the quantities of IH-CO* and IH-NCO* products (Figure 1C, lanes 13-17; Figure 1E, right panels).

Next, we determined the effects of *mer3*Δ, *zip1*Δ, *zip4*Δ, *mms4*Δ, and P_{CLB2}-*SRS2* on the numbers of IH-CO* and IH-NCO* at the *HL**-*SNP+* hotspot in wild-type and *rad51-II3A* (or *rad54*Δ) hybrid zygotes, respectively (Figure 1D). Although the quantities of IH-NCO* were not significantly affected by these five mutants (Figure 1F, lower panels), the numbers of IH-CO* were significantly reduced by *zip1*Δ and *zip4*Δ, slightly reduced by *mer3*Δ, but not affected by *mms4*Δ or P_{CLB2}-*SRS2* (Figure 1F, upper panels).

Consequently, we conclude that class I (ZMM-dependent) IH-COs and IH-NCOs seem to be generated normally by both wild-type and *rad51-II3A* (or *rad54*Δ) SK1/S288c-*HL**-SNP+ hybrid zygotes. Therefore, the hybrid sterility caused by *rad51-II3A* (or *rad54*Δ) is unlikely to be caused by an insufficiency of IH-HR products at the *HL**-*SNP+* DSB hotspot.

P_{CLB2}-*MSH2* results in more IH-HR products at the *HL*-SNP+* DSB hotspot in *zmm*Δ SK1/S288c-*HL*$^{\#}$-SNP+ hybrid zygotes

P_{CLB2}-*MSH2* could rescue (at least in part) the low fertility phenotypes of the four *zmm*Δ (*mer3*Δ, *zip1*Δ, *zip4*Δ and *msh4*Δ) SK1/S288c-*HL**-SNP+ hybrid zygotes but not those of *zip3*Δ or *mms4*Δ SK1/S288c-*HL**-SNP+ hybrid zygotes. The respective order of spore viability is: wild-type (74.5±9.4%) ~ P_{CLB2}-*MSH2* (70.3±10.1%) ~ *zip4*Δ P_{CLB2}-*MSH2* (50.6±16.2%) ~ *zip3*Δ (48.6%±7.2%) ~ *msh4*Δ P_{CLB2}-*MSH2* (42.6±11.8%) ~ *mer3*Δ P_{CLB2}-*MSH2* (40.7±9.0%) ~ *zip1*Δ P_{CLB2}-*MSH2* (35.6%±14.5%) ~ *zip3*Δ P_{CLB2}-*MSH2* (34.7%±0%) ~ *msh4*Δ (30.6±6.9%) ~ P_{CLB2}-*MMS4* (29.2±6.4%) ~ P_{CLB2}-*MMS4* P_{CLB2}-*MSH2* (20.8±7.3%) ~ *zip4*Δ (no tetrads) ~ *zip1*Δ (no tetrads) ~ *mer3*Δ (no tetrads) ~ *mms4*Δ (no tetrads) ~ *mms4*Δ P_{CLB2}-*MSH2* (no tetrads) (Figures 2D, S3-S4, and DS2). Addition of P_{CLB2}-*SGS1* into the *zip4*Δ P_{CLB2}-*MSH2* SK1/S288c-*HL**-SNP+ hybrid zygotes slightly increased spore viability from 50.6±16.2% to 67.6±75.6% (DS2).

Next, Southern hybridization revealed that introducing P_{CLB2}-*MSH2* into *mer3*Δ (Figure 3) and the other four *zmm*Δ (*zip1*Δ, *zip3*Δ, *zip4*Δ and *msh4*Δ; Figures S4) mutants increased IH-NCO* and/or IH-CO* products at the *HL**-*SNP*+ hotspot in the SK1/S288c-*HL**-*SNP*+ hybrid zygotes. In contrast, wild-type, P_{CLB2}-*MSH2*, *mms4*Δ and *mms4*Δ P_{CLB2}-*MSH2* SK1/S288c-*HL**-*SNP*+ hybrid zygotes produced similar quantities of IH-CO* and IH-NCO* products (Figure S5C-D). $DiBAC_4(5)$ and DAPI staining data revealed that ~80% wild-type and P_{CLB2}-*MSH2* SK1/S288c-*HL**-*SNP*+ hybrid zygotes generated tetrads and completed MI. In contrast, *mms4*Δ reduced the capability of both wild-type and P_{CLB2}-*MSH2* SK1/S288c-*HL**-*SNP*+ hybrid zygotes to sporulate, complete MI, and produce viable spores (Figures S5E-F). Thus, only the ZMM proteins, but not the Mms4•Mus81 endonuclease complex, exhibit anti-MMR activities.

Genome-wide quantities of IH-CO and IH-NCO products in wild-type and *rad51-II3A* SK1/S288c-*HL-SNP*+ tetrads with four viable spores

Both the number and position of chromosome-wide IH-COs are tightly controlled by the "CO assurance rule" and the "CO interference rule" (1,25,126,127). To examine how *rad51-II3A* results in hybrid sterility, we applied Oxford Nanopore third-generation sequencing (TGS) technology and a home-made bioinformatics pipeline TSETA (TGS to Enable Tetrad Analysis) to compare genome-wide IH-CO and IH-NCO profiles in wild-type and mutant SK1/S288c-*HL**-*SNP*+ hybrid zygotes. TSETA is a versatile tool for genome-wide comparison, mapping and visualization of SNPs, InDels, illegitimate mutations, and IH-HR products before and after single meiotic events. The TSETA viewer allows users to instantaneously and continuously visualize all 16 near-complete chromosomes at scales ranging from individual nucleotides to full-length chromosomes (85,125,128-131).

In brief, four viable spores were isolated by microdissection from the corresponding hybrid zygotes. After germination and vegetative growth, high-quality genomic DNA was purified from the corresponding progeny and subjected to Oxford Nanopore long-read sequencing. As the recommended sequencing depth to generate a high-quality near-complete genome from long-read data varies depending on sequencing type, with 30–50× coverage recommended for Nanopore (132), the sequencing outputs of all haploid strains in this study are 52.7–139.9x (DS3). Next, we applied the "tetrad" mode of TSETA to align and compare the near-complete genome sequences of the two parental haploid strains and the four F1 progeny haploid strains germinated from the corresponding viable spores. We found that the four wild-type tetrads and the four *rad51-II3A* SK1/S288c-*HL**-*SNP*+ tetrads generated 67.0±3.5 and 57.8±6.2 IH-CO products and 47.5±10.0 and 49.5±6.5 IH-NCO products, respectively (DS3).

It was reported previously that one potential caveat with genome-wide sequencing analysis is that IH-CO values may be overestimated due to selection bias because spore viability is reduced

in the mutants and only tetrads in which all four spores are viable are used (90). For example, wild-type SK1/S288 hybrid zygotes generated more viable spores than *dmc1*Δ *hed1*Δ and *dmc1*Δ *hed1-3A* hybrid zygotes (90). *Hed1-3A* encodes a phosphorylation-defective Hed1 mutant, in which the Thr40, Thr41 and Ser42 residues are all substituted with alanine (A) so that the protein cannot be phosphorylated by Mek1 (90). That previous study deployed next-generation sequencing (NGS) using an Illumina HiSeq 2500 instrument to perform genome-wide mapping (with paired-end reads of 150 X 150 bp) of IH-CO and IH-NCO products in 20 wild-type, 12 *dmc1*Δ *hed1*Δ and 12 *dmc1*Δ *hed1-3A* tetrads obtained from SK1/S288c hybrid zygotes. The results revealed little or no effect on the total number of IH-COs between these three types of hybrid zygotes, though IH-NCO events were significantly reduced in *dmc1*Δ *hed1*Δ (90). Previously, we subjected the same NGS reads (90) to TSETA to assemble the corresponding near-complete haploid genome sequences before and after single meiotic events, as well as for genome-wide mapping of IH-CO and IH-NCO products in the 20 wild-type and 12 *dmc1*Δ *hed1*Δ tetrads obtained from the SK1/S288c hybrid zygotes (85). We found that the wild-type and *dmc1*Δ *hed1*Δ tetrads generated similar average numbers of IH-CO and IH-NCO products (85). Moreover, both the median length of GC tracts (~1000 bp) associated with all IH-HR products and the median density of allelic point disparities (APDs, representing the sum of SNPs and InDels) per CO product (~4.8 APDs per 1,000 bp) in both wild-type and *dmc1*Δ *hed1*Δ hybrid zygotes proved to be nearly identical (85).

In conclusion, the results of these genome-wide sequencing experiments, like those from physical analysis at the *HL***-SNP+* hotspot, cannot explicitly explain why *rad51-II3A* and *dmc1*Δ *hed1*Δ cause hybrid sterility.

The infertility of S288c/SK1 hybrid zygotes with anti-MMR mutations and wild-type N17/SK1 hybrid zygotes is not due to insufficient IH-HR

For meiotic cells unable to form tetrads or produce fertile gametes or viable spores, it is not possible to accurately quantify chromosome-wide IH-HR products using current experimental methods, such as classical genetics, whole-genome sequencing (see above), or immunocytology. In the latter scenario, several "CO designation" protein markers (e.g., *S. cerevisiae* Zip3 and Mlh3, *Caenorhabditis elegans* COSA-1, mouse and *Arabidopsis thaliana* MLH1) can be detected as fluorescent foci along a chromosome under microscopy (45,110,133-135). Although these immunocytological methods do not require genetic markers and can be used in mutants that do not complete meiosis and/or sporulation, concerns have been raised about differences in immunocytological and genetic interferences. For example, several *S. cerevisiae* mutants (e.g., *zip1*Δ, *sgs1*Δ, and *msh4*Δ) show cytological interference but no genetic interference (46). In this study, we also report that P_{CLB2}-*MSH2* could partly rescue the spore viability defects of *zmm*Δ SK1/S288c-*HL*$^{\#}$-SNP+ hybrid zygotes, yet not those of P_{CLB2}-*mms4* and *mms4*Δ SK1/S288c-*HL**-SNP+ hybrid zygotes (Figures 2, S4 and S5). Thus, ZMM-independent IH-COs (in the *zmm*Δ hybrid zygotes) might be inhibited by the Msh2-containing MMR complexes.

We overcame the problem of low spore viability by using a spore-autonomous fluorescence system with three pairs of heterozygous alleles on chromosome VIII (111). The purebred zygotes were generated by sexually crossing SK1(*a, VIII, rgC*) with SK1(*α, VIII, RGc*) (111). The fluorescent protein markers in the resulting zygotes allow direct visualization of inheritance patterns in intact yeast tetrads, eliminating the need for microdissection and permitting meiotic segregation patterns to be ascertained even in aneuploid spores. The length of the *CEN8-ARG4-THR1* interval (~54.9 kb) on chromosome VIII is much longer than that of the *HIS4*::*LEU2-URA3*

interval (~12.0 kb) on chromosome III (30), so it is more suitable for accurately quantifying chromosome-wide CO frequency and CO interference. To study hybrid meiosis, we constructed two hybrid zygotes. The intraspecies hybrid zygotes were generated by sexually crossing S288c(*a, VIII, rgC*) with SK1(*α, VIII, RGc*), whereas the interspecies hybrid zygotes were generated by sexually crossing N17(*a, VIII, rgC*) with SK1(*α, VIII, RGc*) (Figure 4A). The *CEN8-ARG4* (34,040 bp) and *ARG-THR1* (17,684 bp) intervals in the SK1 haploid genome harbor 1.49% (506 bp) and 1.09% (192 bp) SNPs, as well as 2.31% (787 bp) and 2.12% (375 bp) InDels, respectively, relative to those in the S288c haploid genome. In contrast, the *CEN8-ARG4* (34,638 bp) and *ARG-THR1* (17,289 bp) intervals in the *S. paradoxus* reference haploid genome (136) harbor 13.10% SNPs (4,536 bp) and 12.72% SNPs (2,236 bp), as well as 3.79% InDels (1,314 bp) and 5.69% InDels (983 bp), respectively, relative to those in the S288c haploid genome. The stretches of DNA without mismatches within the *CEN8-ARG4-THR1* region are very short (≤120 bp) (DS4).

We confirmed that three purebred zygotes [i.e., SK1(*a, VIII, rgC*)/SK1(*α, VIII, RGc*), N17(*a, VIII, rgC*)/N17(*α, VIII, rgc*), N17(*a, VIII, rgc*)/N17(*α, VIII, rgc*)], as well as the SK1(*α, VIII, RGc*)/S288c(*a, VIII, rgC*) hybrid zygotes, produced >80% viable spores, whereas wild-type N17(*a, VIII, rgC*)/SK1(*α,VIII, RGc*) hybrid zygotes were sterile and hardly produced viable spores (Figure 4B). We also observed that P_{CLB2}-*SGS1* P_{CLB2}-*MSH2* and P_{CLB2}-*SGS1* alone proved slightly more effective in overcoming the interspecies reproductive barrier than P_{CLB2}-*MSH2* (82), P_{CLB2}-*SRS2* or P_{CLB2}-*SRS2* P_{CLB2}-*MSH2* (Figure 4B, Table 1 and DS2). Although wild-type N17(*a, VIII, rgC*)/SK1(*α,VIII, RGc*) hybrid zygotes failed to generate viable spores, >85% of them sporulated, >20% formed tetrads (Figure 4C), and >80% completed MI (Figure 4D).

Next, we quantified the percentages of tetrads exhibiting Mendelian segregation (MS), non-Mendelian segregation (NMS), and MI NDJ. Since IH-NCO (allelic GC) occurs between

heterozygotic sites and result in heteroduplex mismatches that are then recognized and corrected by the MMR system, one of the alleles is converted to the other. This can lead to NMS, i.e., $3^+:1^-$, $1^+:3^-$, $4^+:0^-$, or $0^+:4^-$ alleles in tetrads (based on the four double-stranded DNA duplexes present). The NMS tetrads include all tetrads with ≥1 non-$2^+:2^-$ fluorescent protein markers. The MI NDJ tetrads present two white spores and two black spores under fluorescence microscopy. Although this segregation pattern might also arise from a four-strand double crossing over (DCO) event in the *CEN8-ARG4-THR1* interval, it has been reported previously that the frequency of four-strand DCOs is significantly lower than that of MI NDJ (111). The MS tetrads harbor three $2^+:2^-$ fluorescent protein markers and were used to quantify genetic distances and CO interference [γ = 1 – coefficient of coincidence (c.o.c.)]. Genetic distances were calculated using Perkins equation: cM (centimorgan) = [100 (6NPD + T)] / [2 (PD + NPD + T)], where PD, NPD and T are parental ditype, non-parental ditype, and tetrad type, respectively. Both "genetic distances ± standard errors" and the "NPD ratio" were determined using Stahl Laboratory Online Tools (https://elizabethhousworth.com/StahlLabOnlineTools) (137). The NPD ratio (fN_{obs}/fN_{exp}) is an indication of the intensity of interference between two neighboring genetic markers (i.e., *CEN8* and *ARG4* or *ARG4* and *THR1*), with smaller values indicating stronger positive interference (138,139). The c.o.c. values were calculated by dividing the actual frequency of double recombinants between the *CEN8-ARG4* and *ARG4-THR1* intervals by the expected frequency (https://en.wikipedia.org/wiki/Coefficient_of_coincidence). A positive γ value indicates that the spacing of IH-CO events departs from a random distribution, whereas a negative γ value reflects IH-CO events that are more clustered than the null expectation (Table 1 and DS5-DS7). Below, we discuss the outcomes of these analyses for the different zygote types.

(1) SK1/SK1 purebred zygotes (DS5)

A. The two genetic distances and γ values for the *CEN8-ARG4-THR1* interval are: wild-type zygotes (11.23±0.43 cM, 6.41±0.32 cM and 0.82±0.06, respectively); *rad51-II3A* (11.72±0.51 cM, 6.59±0.41 cM, and γ = 0.77±0.09); *rad54*Δ (11.05±0.48 cM, 6.93±0.40 cM, and γ = 0.84±0.10); P_{CLB2}-*MSH2* (11.48±0.52 cM, 5.85±0.44 cM, and γ = 0.67±0.20); *rad51-II3A* P_{CLB2}-*MSH2* (11.49±0.66 cM, 6.16±0.44 cM, and γ = 0.63±0.14); and *rad54*Δ P_{CLB2}-*MSH2* (11.69±0.49 cM, 6.34±0.39 cM, and γ = 0.50±0.17) (Table 1). Thus, neither *rad51-II3A* nor *rad54*Δ significantly affects genetic distances or CO interference in the SK1/SK1 purebred zygotes. Accordingly, we conclude that the anti-MMR activities of Rad51 and Rad54 are negligible in purebred zygotes as no or very few heteroduplex mismatches will be generated during IH-HR.

B. The insertion of three spore-autonomous fluorescent protein genes into *CEN8, ARG4* and *THR1*, respectively, creates at least three long InDels in the SK1/SK1 hybrid zygotes. We found that P_{CLB2}-*SRS2* (14.65±0.86%) and P_{CLB2}-*MSH2* (14.65±0.86%) resulted in slightly more NMS tetrads than for wild-type (4.88±0.24%), *rad51-II3A* (6.50±1.26%) and *rad54*Δ (7.24±0.93%). P_{CLB2}-*SRS2* slightly increased genetic distances (13.13±0.76 cM and 7.17±0.54 cM) and reduced positive CO interference (γ = 0.25±0.20). The influence of P_{CLB2}-*SRS2* could partly be overturned by *rad51-II3A* (11.60±0.57 cM, 7.14±0.47 cM, and γ = 0.72±0.20), but not by *rad54*Δ (13.45±0.67 cM, 7.59±0.53 cM, and γ = 0.32±0.30). Since the primary function of Srs2 is to remove Rad51 from DSB-associated ssDNA (42), and Rad54 binds tightly to Rad51-ssDNA and acts downstream of Srs2 to promote Rad51-mediated homolog pairing and strand exchange reactions (16), we suggest that Srs2 facilitates the MMR system by antagonizing Rad51's anti-MMR activity. Therefore, yeast Srs2, like its *E. coli* paralog UvrD, belongs to the MMR system.

C. Unlike *zip1*Δ and *zip4*Δ SK1/SK1 purebred zygotes**,** *mer3*Δ and *zip3*Δ purebred zygotes resulted in much lower percentages of mature tetrads for accurate quantification of genetic distances and γ. We found that both *zip1*Δ and *zip4*Δ not only reduced the genetic distances measured in both the *CEN8-ARG4* (4.87±0.42 cM and 1.96±0.38 cM) and *ARG4-THR1* (3.91±0.38 cM and 3.33±0.44 cM) genetic intervals, but also resulted in more NMS tetrads (9.70±3.31% and 13.11±6.59%) and MI NDJ tetrads (7.59±0.30% and 13.50±2.73%). The addition of P_{CLB2}-*MSH2* did not affect the capability of *zip1*Δ and *zip4*Δ SK1/SK1 hybrid zygotes to produce viable spores, but it did increase the genetic distances measured in the *ARG4-THR1* interval (5.38±0.58 cM and 5.06±0.68 cM, respectively) and the percentages of NMS tetrads (16.90±2.77% and 15.78±1.09%, respectively). The order of the respective γ values are: *zip1*Δ (-0.47±0.50) > *zip1*Δ P_{CLB2}-*MSH2* (-3.10±1.37) > *zip4*Δ (-5.27±2.02) ~ *zip4*Δ P_{CLB2}-*MSH2* (-5.45±2.90). Since these four mutant purebred zygotes produced more NMS tetrads compared to wild-type purebred zygotes, it is possible that their negative CO interferences may not only come from DCOs between these two adjacent genetic intervals, but also from a CO in one genetic interval (i.e., *CEN8-ARG4*) and two mutual allelic gene conversion or switching events (i.e., between *THR1* and *THR1::CFP*).

(2) S288c/SK1 hybrid zygotes (DS6)

A. Compared to wild-type SK1/SK1 zygotes, wild-type S288c/SK1 zygotes also displayed similar positive CO interference (γ = 0.60±0.18) and genetic distances (11.49±1.16 cM and 5.85±0.60 cM), but slightly more NMS tetrads (8.54±1.43%). P_{CLB2}-*MSH2*, *rad51-II3A*, *rad54*Δ, and P_{CLB2}-*SRS2* not only reduced positive CO interference, but also increased the percentages of NMS tetrads. P_{CLB2}-*MSH2* (but not P_{CLB2}-*SRS2*) overturned the negative CO interference of both *rad51-II3A* and *rad54*Δ. The order of the γ values is: wild-type (γ = 0.60±0.18) > *rad51-*

II3A P_{CLB2}-*MSH2* (γ = 0.38±0.25) ~ P_{CLB2}-*MSH2* (γ = 0.35±0.10) > *rad54*Δ P_{CLB2}-*MSH2* (γ = 0.07±0.11) > *rad51-II3A* (γ = -0.13±0.13) > *rad51-II3A* P_{CLB2}-*Srs2* (γ = -0.27±0.49) ~ P_{CLB2}-*MSH2* P_{CLB2}-*Srs2* (γ = -0.31±0.21) ~ P_{CLB2}-*SRS2* (γ = -0.31±0.29) ~ *rad54*Δ (γ = -0.37±0.35) > *rad54*Δ P_{CLB2}-*SRS2* (γ = -1.24±0.37). The percentages of NMS tetrads are: wild-type (8.54±1.43%) < P_{CLB2}-*MSH2* (10.09±1.72%) ~ P_{CLB2}-*MSH2* P_{CLB2}-*Srs2* (11.68±0.71%) < *rad54*Δ P_{CLB2}-*MSH2* (14.98±0.50%) ~ *rad51-II3A* P_{CLB2}-*MSH2* (15.71±2.73%) < *rad51-II3A* P_{CLB2}-*Srs2* (19.87±2.67%) ~ P_{CLB2}-*SRS2* (30.56±1.87%) < *rad51-II3A* (38.97±0.34%) < *rad54*Δ (40.30±1.07%) < *rad54*Δ P_{CLB2}-*SRS2* (51.82±2.46%). The percentages of MI NDJ tetrads are: wild-type (0.20±0.10%), P_{CLB2}-*MSH2* (0.10±0.09%), P_{CLB2}-*MSH2* P_{CLB2}-*Srs2*) (0.99±0.00%), *rad54*Δ P_{CLB2}-*MSH2* (0.20±0.20%), *rad51-II3A* P_{CLB2}-*MSH2* (0.07±0.11%) < *rad51-II3A* P_{CLB2}-*Srs2* (0.46±0.30%) ~ P_{CLB2}-*SRS2* (0.99±0.00%), *rad51-II3A* (0.44±0.26%), *rad54*Δ (0.15±0.15%) < *rad54*Δ P_{CLB2}-*SRS2* (0.33±0.57%). These results indicate that the low fertility defects of *rad51-II3A, rad54*Δ, and their double mutants are well correlated with their negative γ values and the percentages of NMS tetrads, but not with the percentages of MI NDJ tetrads. Therefore, the anti-MMR activities of Rad51 and Rad54 can prevent MMR-dependent CO clustering and allelic gene conversion in response to genetic polymorphism.

B. The wild-type, P_{CLB2}-*SGS1*, P_{CLB2}-*MSH2,* and P_{CLB2}-*SGS1* P_{CLB2}-*MSH2* S288c/SK1 hybrid zygotes all generated >76% viable spores, with the two genetic distances being: wild-type (11.44±0.44 cM and 5.87±0.31cM); P_{CLB2}-*SGS1* P_{CLB2}-*MSH2* (13.26±0.77 cM and 5.76±0.55 cM); P_{CLB2}-*MSH2* (14.91±0.60 cM and 6.63±0.50 cM); and P_{CLB2}-*SGS1* (14.46±0.85 cM and 5.61±0.43 cM). The order of the respective γ values is: wild-type (0.60±0.18) > P_{CLB2}-*SGS1* P_{CLB2}-*MSH2* (γ = 0.36±0.16) ~ P_{CLB2}-*MSH2* (γ = 0.35±0.10) > P_{CLB2}-*SGS1* (γ = -0.44±0.69). These results are not only consistent with a previous report that Sgs1 acts downstream of

mismatch recognition by the Msh2-containing MMR complex in hybrid meiosis (80), but they also indicate that Sgs1 can prevent MMR-dependent CO clustering.

The order of NMS tetrad percentages is: wild-type (8.54±1.43%) ~ P_{CLB2}-*MSH2* (10.09±1.72%) ~ P_{CLB2}-*SGS1* (11.29±0.52%) < P_{CLB2}-*SGS1* P_{CLB2}-*MSH2* (29.42±2.83%). Thus, the Msh2-containing MMR complex and Sgs1 might exert non-overlapping roles in preventing allelic switching in S288c/SK1 hybrid zygotes (also see below). Neither the Msh2-containing MMR complex nor Sgs1 significantly affected MI NDJ during S288c/SK1 hybrid meiosis because the percentages of MI NDJ tetrads are: wild-type (0.20±0.10%) ~ P_{CLB2}-*MSH2* (0.10±0.09%) ~ P_{CLB2}-*SGS1* (0.40±0.40%) ~ P_{CLB2}-*SGS1* P_{CLB2}-*MSH2* (0.07±0.11%).

The four *zmm*Δ (*mer3*Δ, *zip1*Δ, *zip3*Δ, and *zip4*Δ) S288c/SK1 hybrid zygotes did not produce enough mature spores to accurately quantify spore viability, genetic distances or CO interference. Although more mature tetrads and viable spores were generated upon introducing P_{CLB2}-*MSH2* into these four *zmm*Δ hybrid zygotes, only the *zip4*Δ P_{CLB2}-*MSH2* hybrid zygotes produced a sufficient number of mature tetrads to enable accurate quantification of genetic distances and CO interference.

The respective spore viability is: *zip4*Δ SK1/SK1 purebred zygotes (33.8±9.0%); *zip4*Δ P_{CLB2}-*MSH2* SK1/SK1 purebred zygotes (36.6±0.8%); and *zip4*Δ P_{CLB2}-*MSH2* S288c/SK1 hybrid zygotes (31.0±3.5%). The respective percentages of NMS and MI NDJ tetrads are: *zip4*Δ SK1/SK1 purebred zygotes (13.11±6.59% and 13.50±2.72%); *zip4*Δ P_{CLB2}-*MSH2* SK1/SK1 purebred zygotes (15.78±1.09% and 11.68±5.00%); and *zip4*Δ P_{CLB2}-*MSH2* S288c/SK1 hybrid zygotes (17.29±0.89% and 5.35±1.30%). The respective γ values are: *zip4*Δ SK1/SK1 purebred zygotes (γ = -5.45±2.90); *zip4*Δ P_{CLB2}-*MSH2* SK1/SK1 purebred zygotes (γ = -7.24±2.71); *zip4*Δ P_{CLB2}-*MSH2* S288c/SK1 hybrid zygotes (γ = -5.68±1.15); wild-type S288c/SK1 hybrid

zygotes (γ = 0.60±0.18); and wild-type SK1/SK1 purebred zygotes (γ = 0.82±0.06). Notably, the two genetic distances of the *zip4*Δ P_{CLB2}-*MSH2* S288c/SK1 hybrid zygotes are higher than those of the *zip4*Δ and *zip4*Δ P_{CLB2}-*MSH2* SK1/SK1 purebred zygotes, i.e., *zip4*Δ SK1/SK1 purebred zygotes (1.96±0.38 cM and 3.33±0.44 cM); *zip4*Δ P_{CLB2}-*MSH2* SK1/SK1 purebred zygotes (2.74±0.49 cM and 5.06±0.68 cM); *zip4*Δ P_{CLB2}-*MSH2* S288c/SK1 hybrid zygotes (8.9±0.9 cM and 10.31±1.03 cM); wild-type S288c/SK1 hybrid zygotes (11.44±0.44 cM and 5.87±0.31cM); and wild-type SK1/SK1 purebred zygotes (11.23±0.43 cM and 6.41±0.32 cM).

(3) N17/SK1 hybrid zygotes (DS7)

A. The haploid genome sequences of N17 and SK1 differ by ~12% (82). The wild-type N17(*a, VIII, rgC*)/SK1(*α, VIII, RGc*) hybrid zygotes displayed highly negative interference (γ = -7.32±2.82) and produced 64.31±1.60% NMS tetrads, 19.42±1.51% MI NDJ tetrads, and only 16.27±0.41% MS tetrads.

B. P_{CLB2}-*SGS1* and P_{CLB2}-*SGS1* P_{CLB2}-*MSH2* proved more effective than P_{CLB2}-*MSH2* (82), P_{CLB2}-*SRS2,* and P_{CLB2}-*MSH2* P_{CLB2}-*SRS2* in breaking the interspecies reproductive barrier, with the order of spore viability being P_{CLB2}-*SGS2* P_{CLB2}-*MSH2* (13.9±5.6%) > P_{CLB2}-*SGS1* (10.2±2.9%) > P_{CLB2}-*MSH2* (5.6±6.1%) ~ P_{CLB2}-*MSH2* P_{CLB2}-*SRS2* (4.9±1.1%) > P_{CLB2}-*SRS2* (1.4±1.4%) ~ wild-type (1.4±2.4%). These results are consistent with our hypothesis that Srs2 and Sgs1 act upstream and downstream, respectively, of the MMR system in the response to genetic polymorphism.

The respective percentages of MI NDJ and NMS tetrads are: wild-type (19.42±1.51% and 64.31±1.60%); P_{CLB2}-*MSH2* (14.55±4.03% and 51.95±15.38%); P_{CLB2}-*SGS1* (20.51±1.02% and 30.80±6.44%); P_{CLB2}-*SGS1* P_{CLB2}-*MSH2* (21.53±2.60% and 35.50±4.79%); P_{CLB2}-*SRS2* (20.79±1.37% and 49.53±2.66%); and P_{CLB2}-*MSH2* P_{CLB2}-*SRS2* (12.65±0.36% and

57.58±5.17%). The respective two genetic distances are: wild-type (7.28±1.71 cM and 8.61±1.59 cM); P_{CLB2}-*MSH2* (8.86±1.21 cM and 16.28±1.37 cM); P_{CLB2}-*SGS1* (2.05±0.29 cM and 23.89±0.81 cM); P_{CLB2}-*SGS1* P_{CLB2}-*MSH2* (5.11±0.58 cM and 26.79±1.10 cM); P_{CLB2}-*SRS2* (16.36±2.03 cM and 25.84±2.47 cM); and P_{CLB2}-*MSH2* P_{CLB2}-*SRS2* (10.06±1.71 cM and 18.09±2.16 cM). The respective γ values are: wild-type (-7.32±2.82); P_{CLB2}-*MSH2* (-1.69±0.60); P_{CLB2}-*SGS1* (-0.33±0.30); P_{CLB2}-*SGS1* P_{CLB2}-*MSH2* (-0.20±0.39); P_{CLB2}-*SRS2* (-2.21±0.30); and P_{CLB2}-*MSH2* P_{CLB2}-*SRS2* (-2.54±0.62). Accordingly, higher percentages of NMS tetrads (allelic switching) and negative CO interference (CO clustering) seem to be more relevant to spore viability than genetic distances and the percentages of MI NDJ tetrads. Since a higher percentage of NMS tetrads indicates a higher frequency of allelic gene conversion, high negative CO interference may not only be caused by adjacent DCOs but also by excessive allelic switching. Either way, our results support the notion that interspecies hybrid infertility is caused by redundant (rather than insufficient) IH-HR.

Allelic disruption (i.e., mutation and deletion) frequently occurs in N17/SK1 hybrid zygotes

It is plausible that excessive allelic switching in the N17(*a, VIII, rgC*)/SK1(*α, VIII, RGc*) hybrid zygotes may be caused by allelic heterozygosity, i.e., the long InDels caused by integration of the three fluorescent protein maker genes. Consequently, we constructed a N17(*a, VIII, rgC*)/SK1(*α, VIII, rgC*) hybrid strain in which the same spore-autonomous *CFP* gene is integrated into the *THR1* loci of both N17(*a, VIII, rgc*) and SK1(*α, VIII, rgc*) (Figure 6A), with a spore viability of 1.4±2.4% (wild-type) and 10.2±2.9% (P_{CLB2}-*SGS1*) (Figure 6B). Only 37.5±6.6% wild-type and 26.3±3.5% P_{CLB2}-*SGS1* N17(*a, VIII, rgC*)/SK1(*α,VIII, rgC*) hybrid zygotes followed Mendel's law and generated 4^{+}:0^{-} tetrads, i.e., four cyan fluorescent spores. Wild-type and P_{CLB2}-*SGS1*

N17(*a,rgC*)/SK1(*α,rgC*) hybrid zygotes also produced many NMS tetrads, i.e., 19.4±2.4% and 22.9±3.4% 3^+:1^- tetrads, 40.3±4.4% and 35.6±5.7% 2^+:2^- tetrads, 2.9±0.8% and 8.3±3.5% 1^+:3^- tetrads, and 3.2±2.0% and 5.1±2.9% 0^+:4^- tetrads, respectively (Figure C and DS8). These NMS tetrads might result from IH-HR-induced allelic mutations or from allelic loss caused by NDJ during MI or MII. Accordingly, we postulate that the infertility displayed by N17/SK1 interspecies hybrids is due to excessive IH-HR, which induces allelic disruption (i.e., mutation and loss) within chromosomal regions containing genes indispensable for spore germination or vegetative growth.

To rule out the possibility that excessive IH-HR and high NMS events only occur within the *CEN8-ARG4* and *ARG4-THR1* intervals, we constructed another interspecies hybrid diploid strain, i.e., N17(*a, IV, rcG*)/S288c(*α, IV, RCg*), with three spore-autonomous fluorescent maker genes integrated into chromosome IV. In brief, *RFP*, *CFP* and *GFP* were integrated next to *YDR042C*, *YDR199W* and *YDR403W*, respectively. The lengths of the *YDR042C::RFP-YDR199W::CFP* and *YDR199W::CFP-YDR403W:GFP* genetic intervals are ~313 kilobasepairs (kbp) and ~421 kbp, respectively (Figure S6). We found that, like N17(*a, VIII, rgC*)/SK1(*α, VIII, RGc*), the N17(*a, IV, rcG*)/S288c(*α, IV, RCg*), hybrid strain not only experienced NMS more frequently than MS or MI NDJ, but also exhibited negative CO interference (Table 1and DS9).

DISCUSSION

Herein, we report that the MMR system and the HR machinery display a dynamic yin-yang relationship in the response to different levels of genetic polymorphism, e.g., SK1/SK1 purebred zygotes and the S288c/SK1 and N17/SK1 hybrid zygotes. The MMR system and the HR machinery antagonize each other in meiosis, as several HR proteins (e.g., Rad51, Rad54, Mer3,

Zip1, the ZZS complex, and MutSγ) possess anti-MMR activities. Our results have also indicated that, in response to genetic polymorphism, excessive (rather than inadequate) IH-HR recombination products are generated in interspecies *S. cerevisiae*/*S. paradoxus* hybrid zygotes and in intraspecies S288c/SK1 hybrid zygotes with anti-MMR mutations. This finding is consistent (at least in part) with a recent report that Msh2 stimulates interfering IH-COs and inhibits non-interfering IH-COs in response to genetic polymorphisms in higher plant *A. thaliana* (140).

Our results also provide several new insights into the roles of various HR proteins in hybrid meiosis. First, Rad51 and Dmc1 utilize different mechanisms to encounter heteroduplex mismatches and the MMR system during homology-directed DSB repair. Dmc1 and Tid1 (Rdh54) do not possess anti-MMR activities, and Dmc1 is superior to Rad51 in tolerating heteroduplex mismatches before either is recognized by the Msh2-containing MMR complexes. In contrast, Rad51-ssDNA filaments act together with Rad54 to antagonize the MMR system after mismatch recognition. This hypothetical model can explain the finding of a previous report that *S. cerevisiae* Rad51 and Dmc1 exhibit similar mismatch tolerability during homology pairing strand exchange *in vivo* (114). Second, the anti-MMR activity of Rad51 preferentially acts against Msh2-mediated mismatch recognition and MutLα-mediated mismatch correction rather than MutLγ-mediated joint molecule resolution. Third, Rad54 acts downstream of Srs2 and Rad51 to antagonize the MMR system. The anti-MMR activity of Rad54 prevails over Rad54's pro-HR activity in hybrid meiosis. Fourth, like its *E. coli* paralog UvrD, Srs2 is an MMR protein that disassembles Rad51 from the Rad51-ssDNA nucleoprotein filament. Fifth, Sgs1 acts after MMR-mediated mismatch recognition to facilitate MMR-induced negative CO interference (CO clustering) and allelic gene conversion. Accordingly, P_{CLB2}-*SGS1*, alone or together with P_{CLB2}-*MSH2*, breaks the interspecies reproductive barrier by reducing CO clustering and excessive allelic gene conversion. Our

hypothetical model can also explain why suppression of recombination between homeologous sequences was found previously to be enhanced in *srs2* mutants but reduced in *sgs1* mutants (84). Sixth, in the absence of the SC (i.e., *zip4*Δ), the Msh2-containing MMR system inhibits the formation of ZMM-independent and non-interfering IH-CO products (e.g., at the *HL**-*SNP*+ DSB hot spot) in the SK1/S288c-*HL**-*SNP*+ hybrid zygotes.

In conclusion, our results indicate that hybrid infertility is in fact due to a yin-yang imbalance between MMR and HR. In other words, MMR takes precedence over HR when the level of genetic polymorphism is high (e.g., N17/SK1 and N17/S288c hybrid zygotes) or when the anti-MMR function of the HR machinery is defective (e.g., S288c/SK1 hybrid zygotes with anti-MMR mutations). In this scenario, too many heteroduplex mismatches are recognized by the MMR system, which then recruits Sgs1 to prevent excessive allelic switching. Since allelic switching is highly mutagenic, it might represent one of the major causes of infertility in interspecies hybrid zygotes.

It is intriguing to point out that meiosis-induced hypermutations (including C→T and not C→T mutations) were reported previously in crosses of two highly inbred *Neurospora crassa* strains (141), as well as in crosses of two *Trichoderma reesei* wild isolates with highly diverse genome sequences (85,128,130). The majority of C→T mutations in *N. crassa* and *T. reesei* occur premeiotically via repeat-induced point mutation (RIP), a fungus-specific genome defense mechanism that mitigates the deleterious consequences of repeated genomic regions and transposable elements (TEs) via cytosine methylation and deamination (142-144). Notably, in crosses of two highly inbred *N. crassa* strains, RIP is also associated with an elevated rate of mutation outside of classical RIP zones. These RIP-associated, non-classical mutations account for the majority of coding DNA sequence (CDS) mutations throughout the sexual cycle (141). In

contrast, we have shown previously that many C→T and not C→T mutations in crosses of two *T. reesei* wild isolates with highly diverse haploid genome sequences not only occur outside of classical RIP zones, but are also non-RIP-associated (85,125,128). Further investigations will reveal if the phenomena we have described in this report can account for the non-RIP-associated mutations induced by *T. reesei* hybrid meiosis.

Although the spore autonomous fluorescent method is superior to several other experimental approaches (e.g., classical genetics, genome-wide sequencing, physical analysis, and cytology) for accurate quantification of genetic distance, CO interference and/or allelic switching, we acknowledge that this approach has several potential drawbacks. First, only tetrads (but not dyads and triads) were used to quantify genetic distances and CO interference, as it is difficult to quantify IH-HR products in meiotic cells that do not sporulate well (i.e., monads, dyads or triads). Second, both interspecies hybrid zygotes and intraspecies hybrid zygotes with anti-MMR mutations produce high percentages of NMS tetrads, so further investigations are needed to establish if DCO events that cause negative CO interference are indeed attributable to two authentic IH-CO products. Furthermore, our results cannot rule out the possibility that DCOs may be caused by allelic switching events. In the latter case, negative CO interference will not lead to the closely-spaced chiasma that reduce sister chromatin cohesion and tension, leading to MI NDJ. This is an intriguing hypothesis because it may explain why some "observed" IH-COs cannot form chiasma and are non-interfering.

DECLARATIONS

Ethics approval and consent to participate

Not applicable.

Consent for publication

All authors have read and approved of its submission to this journal.

Data availability

All relevant data are within the paper and its Supporting information files.

Conflicts of Interest

The authors declare no conflicts of interest.

Funding

This work was supported by intramural fund of the Institute of Molecular Biology, Academia Sinica, Taiwan and Academia Sinica, Taiwan, Republic of China (AS-GCS-114-L05).

Acknowledgment

We thank the Imaging Core Facility of the Institute of Molecular Biology, Academia Sinica, for technical support, John O′Brien for English editing, Matthew Neale (University of Sussex, UK) for sharing the PCR-based P_{CLB2}-*HA::KanMx4* integration plasmid, Scott Keeney (HHMI and Sloan Kettering Institute, USA) for sharing the SK1 strains and/or integration plasmids with three spore-autonomous fluorescence markers, Valérie Borde for sharing both *zip2*-Δ*XPF* and *zip4-N919Q* mutants, Eric Alani (Cornell University) for sharing the *sgs1*Δ-C795 mutant, Duncan Greig (University College London), Jasmine Ono (University of Nottingham) and Jun-Yi Leu (IMB,

Academia Sinica) for sharing *S. paradoxus* N17 and *S. cerevisiae* S288c strains, Valérie Borde (Institut Curie, France), Michael Lichten (NIH, USA), Gerry Smith (Fred Hutchinson Cancer Center, USA), and Nancy Kleckner (Harvard University, USA) for their helpful research advice, and Su-Chien Chen and Agatha Cecilia Sihite (IMB, Academia Sinica) for research assistance.

MATERIALS and METHOD

Yeast strains and cultures

Standard methods were deployed for the growth and genetic manipulation of yeast (145). Unless noted otherwise, *S. cerevisiae* (85,92) and *S. paradoxus* (82) strains were grown at 30 °C in YPD medium (1% yeast extract, 2% peptone, and 2% glucose). KanMX, HphMX, and NatMX cassettes, which confer resistance to G418, hygromycin or nourseothricin, respectively (146), were incorporated into the SK1/SK1 purebred and SK1/S288c hybrid strains. G418, hygromycin, and nourseothricin were added to the media at final concentrations of 200 μg/ml, 300 μg/ml, and 50 μg/ml, respectively (147). All meiotic experiments were performed as described previously (107,148) using SK1/SK1 purebred diploid cells, and S288c/SK1, N17/SK1, or N17/S288c hybrid diploid cells.

Antisera and immunoblotting

The rat anti-HA antibody was purchased from Roche (Basel, Switzerland). The rabbit anti-Hsp104 antisera was kindly provided by Chung Wang (Academia Sinica, Taiwan). In brief, whole-cell extracts of ~6×10^7 yeast vegetative cells and sporulating cells precipitated with trichloroacetic acid (TCA, Sigma-Aldrich), and then subjected to SDS-PAGE and Western blotting as described previously (92). Hsp104 was used as a loading control. Size in kilodaltons of standard protein markers is labeled to the left of the blots. All vegetative haploid and diploid cells were grown at 30 °C in YPDA medium to OD600 to 0.4-0.6. Sporulating cells were grown overnight at 30 °C in YPA medium (1% yeast extract, 2% peptone, and 2% potassium acetate), then transferred into

sporulation medium (2% potassium acetate) at zero time point, and then harvested at indicated time points.

Determination of the percentages of spore viability, post-MI (%) and sporulation efficiency

Spore viability on the dissection plates was assessed after three days of growth, as described previously (92,107,148). To determine post-MI (%), i.e., the percentage of cells that completed MI and both MI+MII divisions (122,123), sporulation cultures of each cross were harvested 24 hours after being transferred into sporulation medium and then divided into three aliquots. The sporulating cells in the first aliquots (1.0 mL) were collected by centrifugation, resuspended in 1.0 mL of fixation solution (40% ethanol and 0.1M sorbitol) at 4 °C, and then stained with 4, 6-diamidino-2-phenylindole (DAPI). DAPI was excited using a 404 nm laser and emission light was collected with 450/50 BP filters. Fluorescence microscopy images of the stained cells were acquired using a Zeiss Axio Imager Z1 fluorescence microscope and a 63x/1.4 oil immersion objective.

To quantify sporulation efficiency, the second aliquot of sporulation cultures remained untreated, and the third aliquot was stained with $DiBAC_4(5)$ [Bis-(1,3-dibutylbarbituric acid) pentamethine oxonol], which can stain yeast tetrads and dyads, as well as adhere to spores following bulk tetrad disruption (121). The vital dye $DiBAC_4(5)$ (Absorption = 590 nm; Emission = 616 nm) is a lipophilic, anionic molecule that is known to fluorescently stain dead yeast cells based on collapse of their membrane potential (149). In brief, sporulating diploid cells were rinsed twice with phosphate-buffered saline (PBS), resuspended in 1 mL PBS, and then stained at room temperature in the dark for 1 minute with 1 μg/mL DiBAC4(5) (Sigma-Aldrich, US) using a 1 mg/mL stock solution in DMSO. After staining, excess dye was removed by rinsing and

resuspending the cells in 1 mL PBS. Flow cytometry was performed on a BD FACSymphony A3 Cell Analyzer, as described previously (150). The cells were diluted in PBS to a density of ~1×10^7 cells/ml and sorted at room temperature using the instrument's "ultrapure" setting. Since yeast diploid cells lacking *DMC1* cannot complete MI and hardly form any dyads or tetrads (151), both non-stained samples and DiBAC4(5)-stained *dmc1*Δ sporulating cells were used for gating.

Genome-wide mapping of interhomolog recombination products generated by wild-type and mutant SK1/S288c hybrid zygotes

We applied Oxford Nanopore Technology (ONT) to sequence genomic DNA. Isolation of genomic DNA, ONT genome sequencing and assembly were carried out as described previously (129-131,144). ONT direct DNA library preparation and sequencing were performed at the Genomics Core of the Institute of Molecular Biology, Academia Sinica. In brief, small fragments of purified genomic DNA were removed by using an Ampure cleanup kit (Beckman Coulter). High-quality DNA quantification was conducted using a Qubit fluorometer (Thermo Fisher Scientific). The average length of genomic DNA was scaled using Femto Pulse (Agilent). We used 1 μg of genomic DNA for library construction. The library contained three or four DNA samples barcoded using the EXP-NBD104 Rapid barcoding kit (Oxford Nanopore Technologies), and adaptors were added with the SQK-LSK109 ligation sequencing kit (Oxford Nanopore Technologies). The library was loaded onto a R9.4.1 Flow Cell system (FLO-MIN106) and processed for 48 hours on the MinION platform. The sequencing process was controlled using MinKNOW software (version 3.6.5; Oxford Nanopore Technologies). All experimental procedures were carried out according to the manufacturer's instructions. FAST5 data files were generated upon completion of sequencing. These files were converted into FASTQ files in Guppy (v3.6.0). All reads were split into separate

FASTQ files based on their barcode by means of the qcat tool (v1.1.0), and then Canu (v2.1.1) (152) was used to perform whole-genome assembly on the corresponding FASTQ files for each sample. The parameter of corOutCoverage was set to 60 based on sequencing read depth. Finally, we used medaka (v1.2.0) to polish the assemblies with the raw reads. The raw datasets have been deposited in the National Center for Biotechnology Information (Bioproject accession number PRJNA1216236). Since Canu generated expected numbers of contigs for each sample, and a comparison of the genome to wild-type QM6a indicated no broken contigs, we did not perform any manual finishing or validation. Genome-wide mapping of interhomolog recombination products was performed using the same approaches described in our previous recombination analyses of *T. reesei* and *S. cerevisiae* hybrid meiosis (85,128,130).

Physical analysis by Southern hybridization of meiotic recombination

Synchronous meiosis was performed as described previously (122,123). Genomic DNA extraction and 1D gel analysis were also performed as described previously (22,147). The Southern blotting physical analysis was carried out using "Probe A", as described previously (153). DNA probes were radiolabeled using a Random Priming kit (Invitrogen, USA) (23). Hybridizing species were quantitated using a Fuji BAS2000 phosphorimager and Image Gauge V3.3 software (Fuji Photo Film Co. Ltd) (125).

Analysis of CO frequencies and interferences

Diploids were sporulated in liquid sporulation medium and the recombination between fluorescence markers on chromosome VIII was scored after 24 hours of sporulation using a Zeiss Axio Imager Z1 fluorescence microscope, as described previously (111). Two independent sets of

each strain were combined and 1515-3460 tetrads were scored for COs in two test intervals and for MI NDJ events. Genetic distances in the *CEN8-ARG4* and *ARG4-THR1* intervals were calculated from the distribution of parental ditype (PD), nonparental ditype (NPD), and tetratype (T) tetrads, and genetic distances (cM) were calculated using Perkins equation: cM (centimorgan) = [100 (6NPD + T)] / [2 (PD + NPD + T)]. Standard errors of genetic distances were calculated using Stahl Laboratory Online Tools (https://elizabethhousworth.com/StahlLabOnlineTools). Interference (γ) is defined as γ = 1 – (coefficient of coincidence or c.o.c.), where c.o.c. is calculated by dividing the actual frequency of double recombinants by the expected frequency (https://en.wikipedia.org/wiki/Coefficient_of_coincidence) (43). Both genetic distances and the "NPD ratio" (fN_{obs}/fN_{exp}) were also calculated using Stahl Laboratory Online Tools (https://elizabethhousworth.com/StahlLabOnlineTools) (137). The NPD ratio is an indication of the intensity of interference, with smaller values indicating stronger positive interference (138,139).

Statistical analysis

We combined three independent sets of each strain and scored tetrads either individually (N/3; split in triplicate) or collectively (i.e., N; total) (DS5-7 and DS9). All quantitative data is shown as mean plus/minus Standard Deviation of the mean (SD), as indicated in each figure legend. Graphs were plotted using GraphPad Prism 10.1.0 (GraphPad software). Statistical analyses were performed using two-way analysis of variance (ANOVA, for comparing genetic distances of wild-type purebred and hybrid strains), one-way ANOVA (for comparing spore viability, γ, and MI NDJ of wild-type purebred and hybrid strains) with Bonferroni's post-test correction or an unpaired t-test. All statistical analyses were performed using Sigmastat 3.5 (SigmaPlot software). P values ≥ 0.05 were considered non-significant.

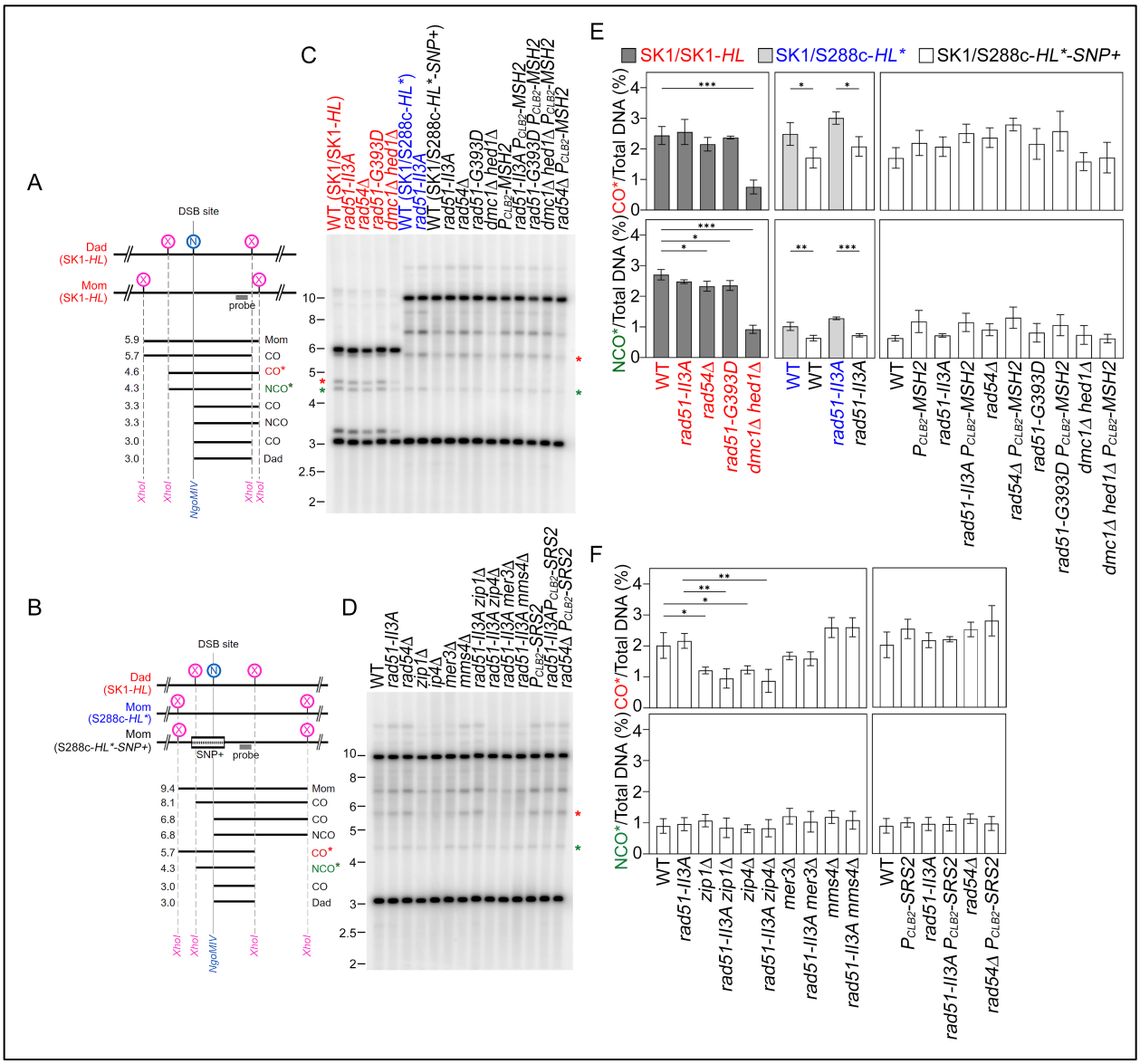

Figure 1. Genetic screening and physical analyses of anti-MMR mutants. (**A,B**) Schematic of the DSB hotspot in SK1/SK1-*HL* purebred zygotes, and SK1/S288c-*HL** and SK1/S288c-*HL**-*SNP*+ hybrid zygotes. The DNA probe used for Southern hybridization is shown as a grey box. *XhoI* and *NgoMIV* are indicated as X and N, respectively. (**C,D**) Physical analysis by Southern hybridization of recombinants at the *HL* and *HL** DSB hotspots. Genomic DNA was isolated 24 hours after the meiotic cells were transferred into sporulation medium and then digested with *XhoI* and *NgoMIV* to detect IH-CO and IH-NCO recombinants. (**E,F**) Quantification of recombinants from three independent timecourses, one of which is shown in C and D. Statistical analyses were performed using one-way ANOVA with Bonferroni's post-test correction. All statistical analyses were performed using Sigmastat 3.5 (SigmaPlot software). *P* values ≥ 0.05 were considered non-significant.

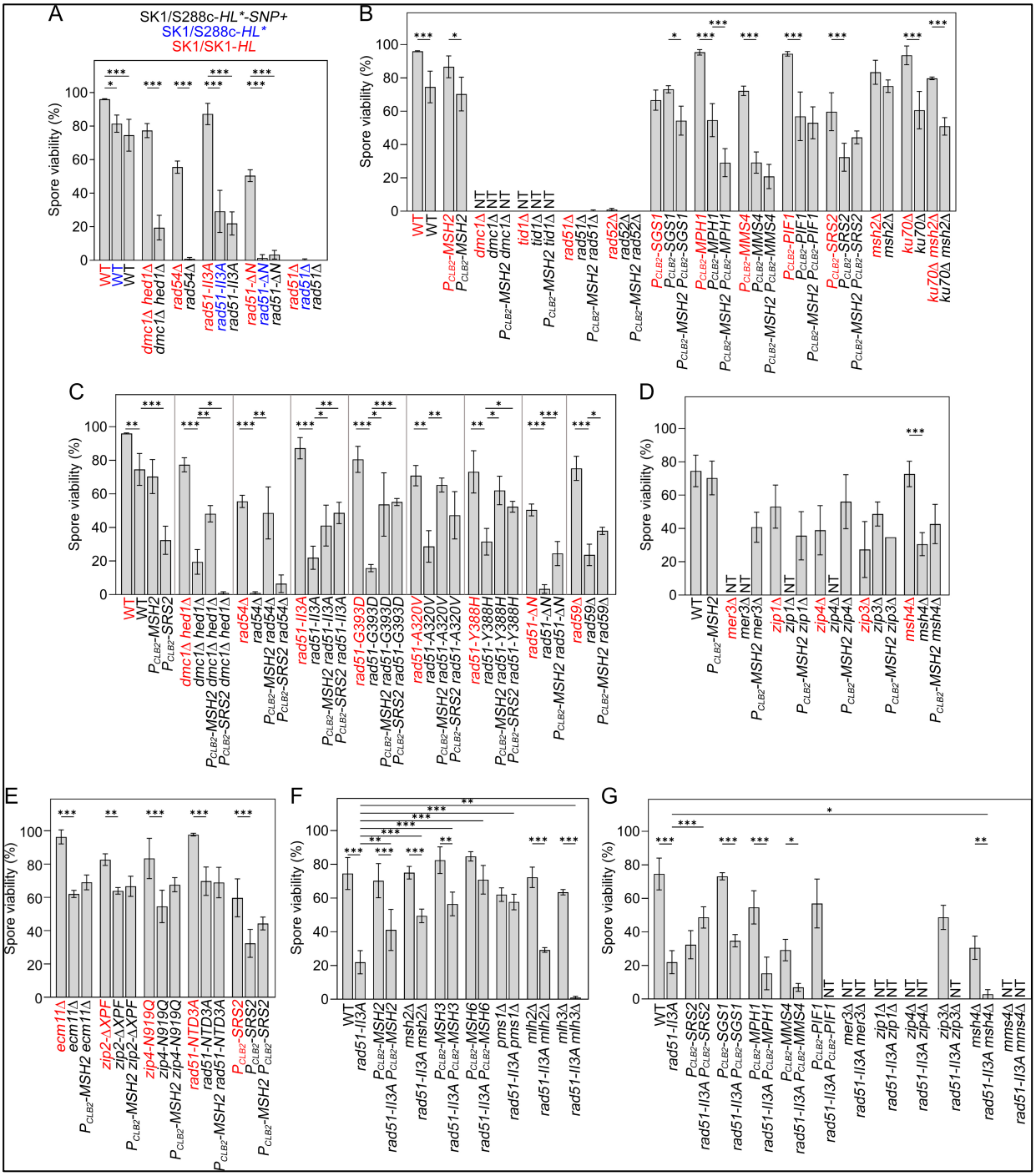

Figure 2. Identification of anti-MMR genes. Yeast strains were transferred into sporulation medium at 30 °C for three days. The tetrads were subjected to limited zymolyase digestion, sufficient to break down the protective membrane surrounding spores. The digested tetrads were transferred onto the surface of an YPDA agar plate on a microscopic platform. Tetrads were selected, picked up, and their individual spores were pulled apart using a micromanipulator device controlling the movement of a fine glass needle. Both the S288c/SK1 hybrid zygotes and the SK1/SK1 purebred zygotes produced >90% viable spores. The anti-MMR mutations (except

*mer3*Δ) resulted in lower fertility (spore viability) in S288c/SK1 hybrid zygotes compared to SK1/SK1 purebred zygotes. The low fertility phenotype of S288c/SK1 hybrid zygotes with anti-MMR mutation(s) could be rescued by P_{CLB2}-*MSH2, msh2*Δ*,* P_{CLB2}-*MSH3,* and/or P_{CLB2}-*MSH6.* All quantitative data are shown as mean values plus/minus standard error of the mean (SEM). Graphs were plotted using GraphPad Prism 10.1.0 (GraphPad software). Statistical analyses were performed using one-way ANOVA with Bonferroni's post-test correction, or an unpaired t-test. All statistical analyses were performed using Sigmastat 3.5 (SigmaPlot software). P values ≥ 0.05 were considered non-significant. NT (no or very few tetrads). ND (not determined).

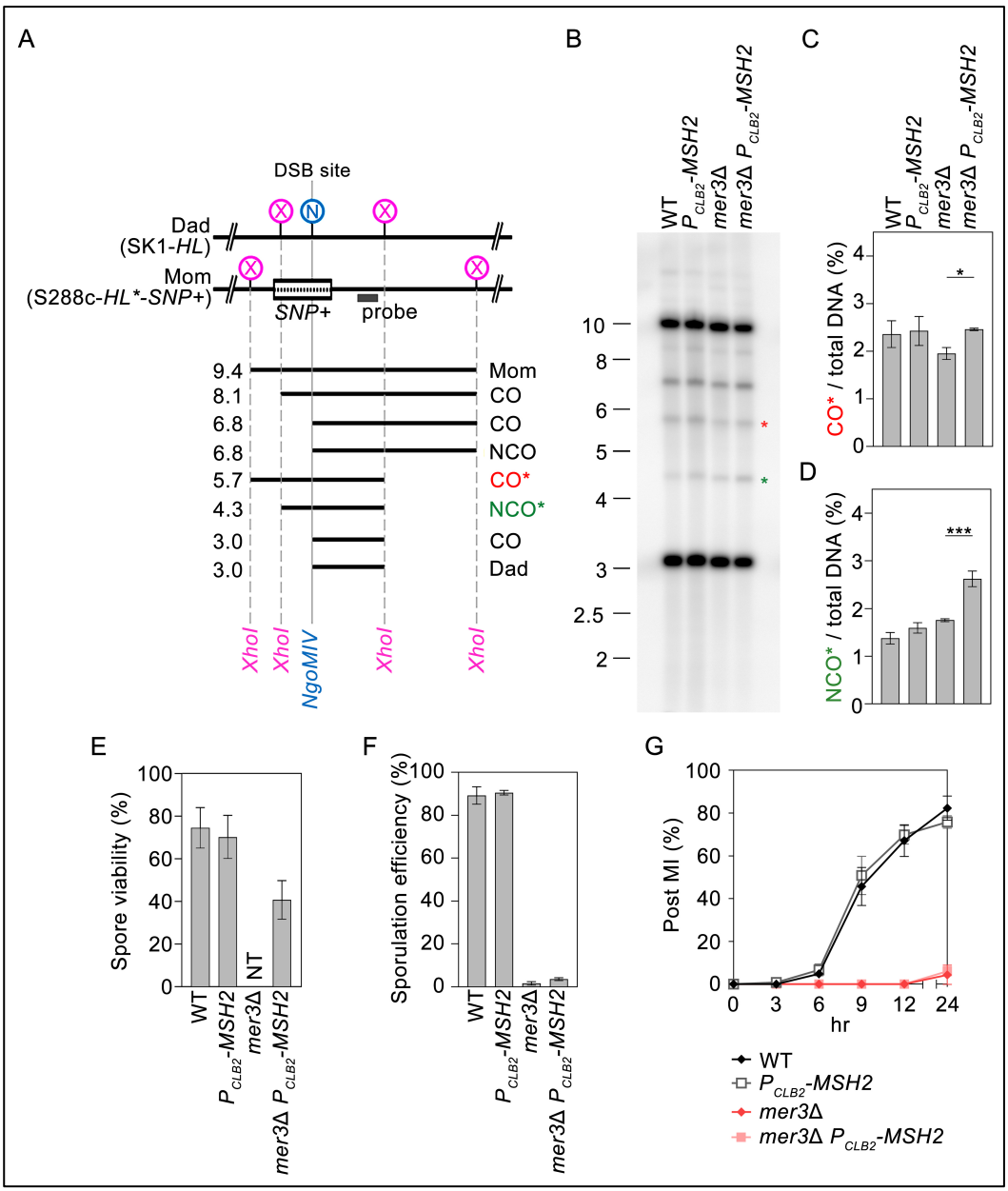

Figure 3. The effect of *P_{CLB2}-MSH2* on *mer3*Δ SK1/S288c-*HL*-SNP+* hybrid zygotes increases spore viability and sporulation efficiency but not the quantities of IH-CO and IH-NCO recombinants at the *HL*-SNP+* DSB hotspot. (**A**) Schematic of the DSB hotspot in the SK1/S288c-*HL*-SNP+* hybrid zygotes. (**B**) Physical analysis by Southern hybridization of recombinants at the *HL* and *HL** DSB hotspots. (**C,D**) Quantification of recombinants from three independent timecourses, one of which is shown in B. (**E**) Spore viability was determined by tetrad analysis. (**F**) Sporulation efficiency was determined by staining the sporulating cells with $DiBAC_4(5)$ [Bis-(1,3-dibutylbarbituric acid) pentamethine oxonol] (121) and analyzed by flow cytometry using a BD FACSymphony A3 Cell Analyzer (150). (**G**) The percentages of cells that completed MI and both MI+MII divisions (Post MI) (122,123) were determined by staining the sporulating cells with 4, 6-diamidino-2-phenylindole (DAPI).

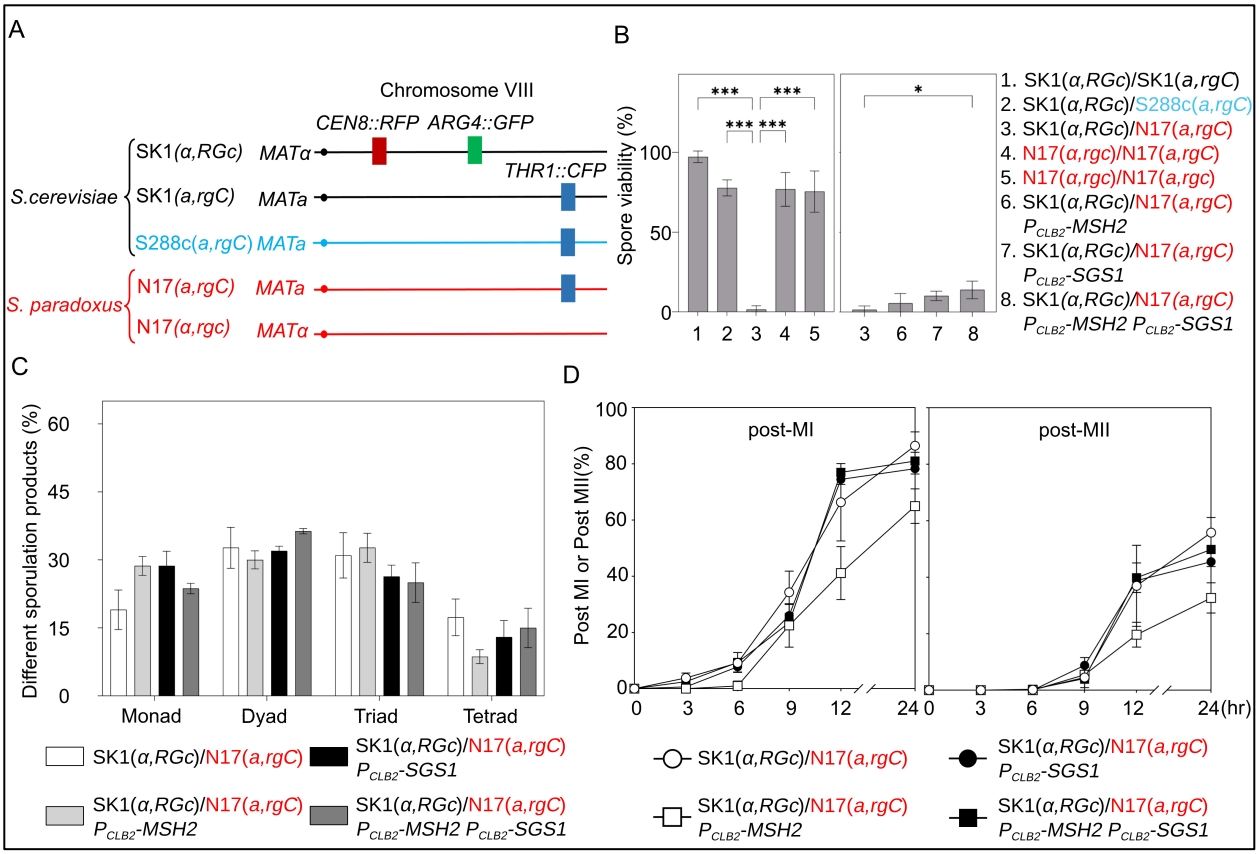

Figure 4. The spore-autonomous fluorescent strains used in this study. (A) Illustration of the spore-autonomous fluorescent set-up on chromosome VIII of *S. cerevisiae* SK1(*MATα*)/SK1(*MATa*) purebred zygotes (111), *S. cerevisiae* S288c(*MATα*)/SK1(*MATa*) intraspecies hybrid zygotes, and interspecies N17(*MATα*)/SK1(*MATa*) hybrid zygotes. *MATa, MATα*, chromosome VIII, *CEN8::RFP*, *CEN8*, *ARG4::GFP*, *ARG4, THR1-CFP* and *THR1* are indicated as *a*, *α*,VIII, *R*, *r*, *G*, *g, C*, and *c,* respectively. (**B**) Spore viability was analyzed after 3 days on sporulation media (2% potassium acetate) at 30 °C. Only tetrads (but not dyads or triads) were microdissected on Yeast Peptone Dextrose (YPD) agar plates to score spore viability. (**C, D**) The majority of *S. cerevisiae*/*S. paradoxus* SK1(*α, VIII, RGc*)/N17(*a, VIII, rgC*) and P_{CLB2}*-MSH2* P_{CLB2}*-SGS1* SK1(*α, VIII, RGc*)/N17(*a, VIII, rgC*) hybrid zygotes can undergo normal meiosis and sporulation. (**C**) Percentages of dyads, triads, and tetrads generated by *S. cerevisiae*/*S. paradoxus* hybrid zygotes after 3 days on sporulation media at 30 °C. Error bars indicate the standard deviation between experiments (*n* = 3). (**D**) Meiotic progression was monitored by DAPI (4′,6-diamidino-2-phenylindole) staining of nuclei. Two hundred cells harvested from sporulation medium having 2-4 nuclei or 3-4 nuclei (as determined by fluorescence microscopy) were assessed as having completed meiosis I (post-MI) and meiosis II (post-MII), respectively. The percentages of such cells over total cells counted per time-point have been plotted (n = 3).

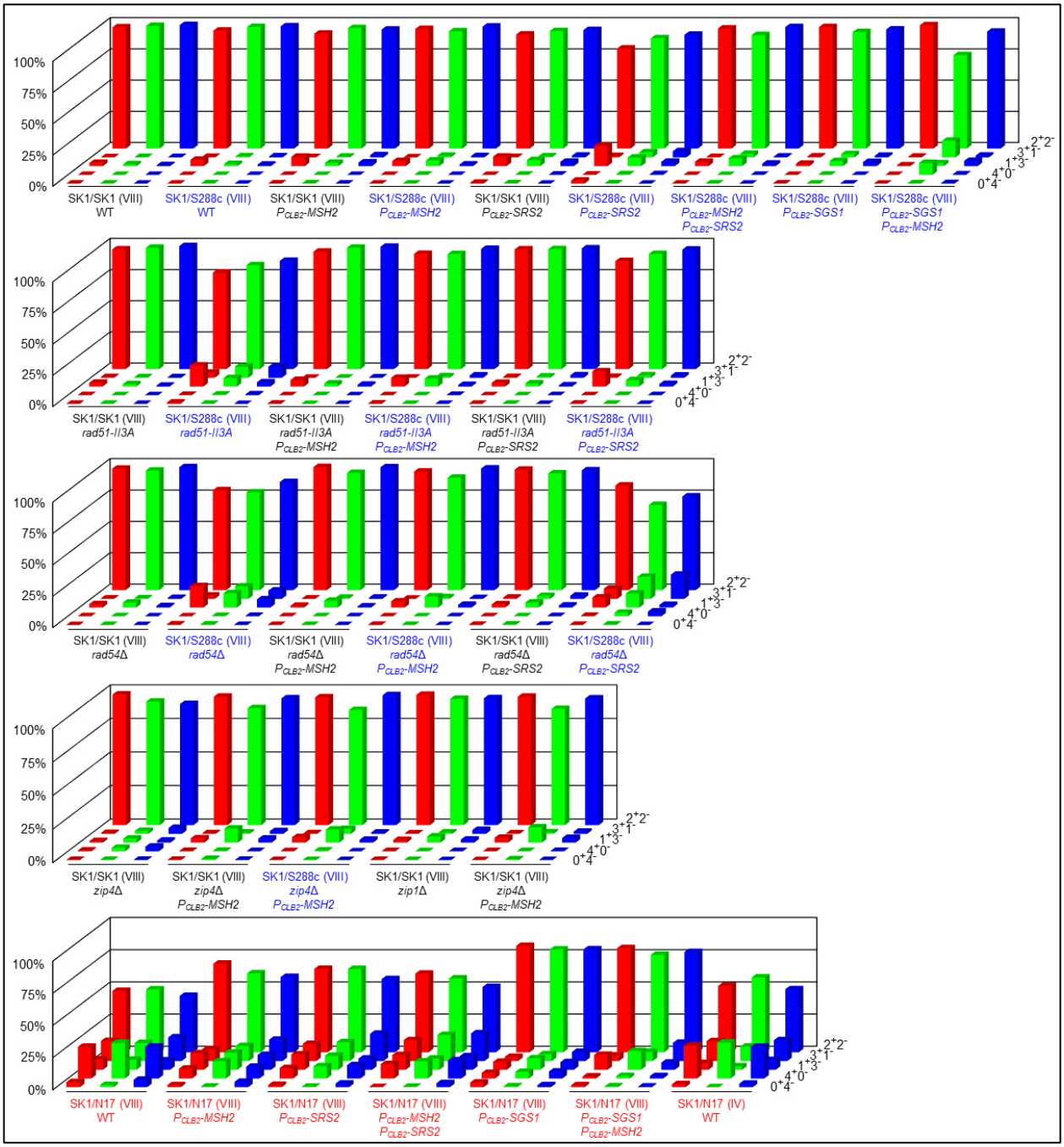

Figure 5. The percentages of tetrads with three heterozygous spore-autonomous fluorescent marker genes that underwent Mendelian segregation (MS; i.e., 2^+:2^-) and non-Mendelian segregation (NMS; i.e., 3^+:1^-, 1^+:3^-, 4^+:0^-, or 0^+:4^-).

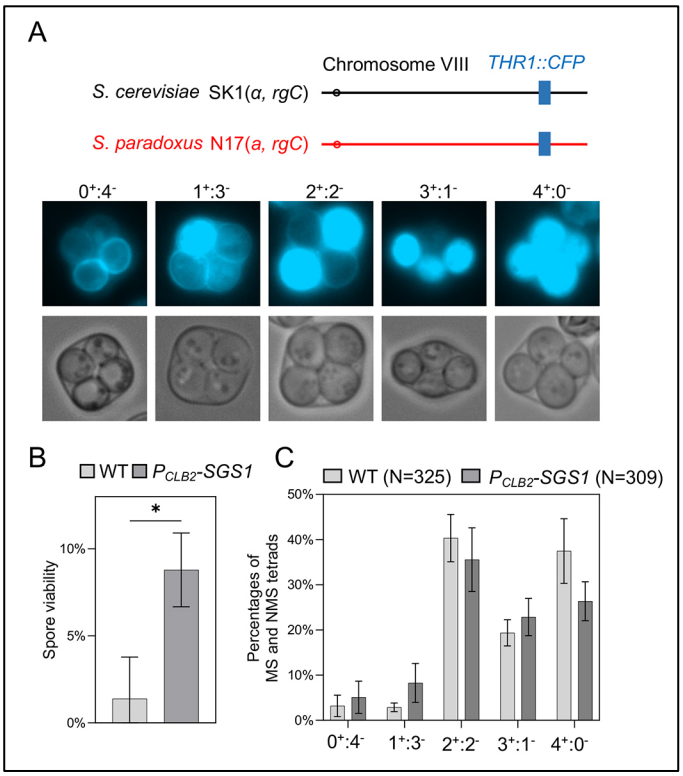

Figure 6. Allelic gene disruption (mutation or loss) frequently occurs in the *S. paradoxus/S. cerevisiae* hybrid zygotes. (**A**) Illustration of the homozygous spore-autonomous-CFP fluorescent gene set-up on chromosome VIII of an interspecies N17(*MATα*)/SK1(*MATa*) hybrid zygote. Representative images of tetrads that underwent Mendelian segregation (MS; i.e., 4^{+}:0^{-}) and non-Mendelian segregation (NMS; i.e., 0^{+}:4^{-}, 1^{+}:3^{-}, 2^{+}:2^{-}, or 3^{+}:1^{-}). (**B**) Spore viability. (**C**) Percentages of MS and NMS tetrads.

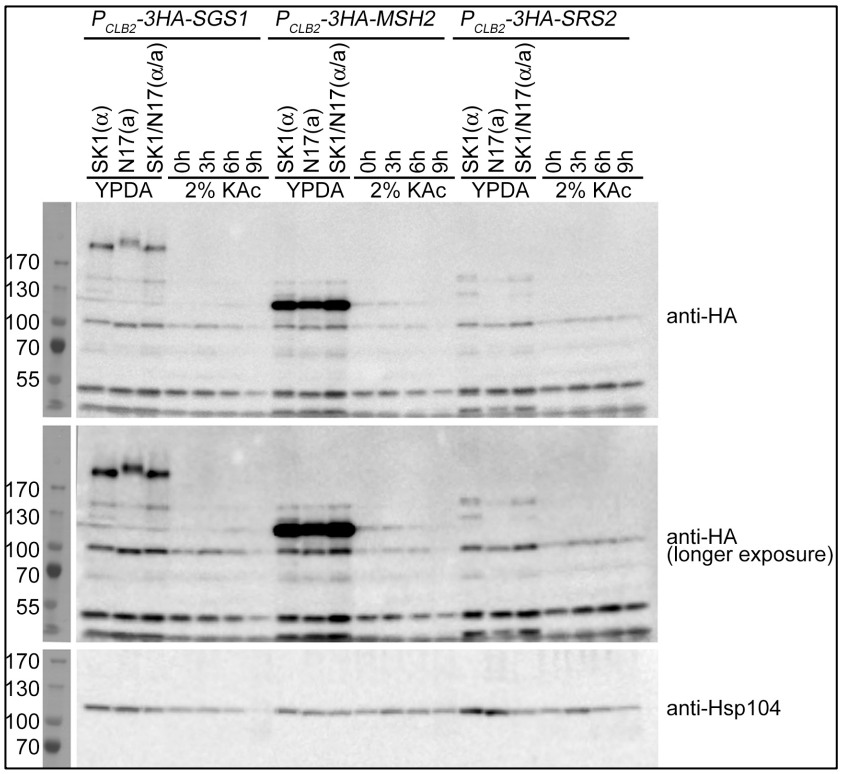

Figure S1. P_{CLB2} represses meiotic expression of *MSH2*, *SGS1* and *SRS2*. whole-cell extracts of ~6 × 10^7 vegetative or sporulating cells were resuspended with 1ml of freshly prepared buffer (0.185 M NaOH, 0.75% β-mercaptoethanol), incubated on ice for 15 min, and mixed with 150 µl of 55% trichloroacetic acid (TCA) for 10 min on ice. The cell suspension was centrifuged at 13,500 rpm for 10 min. The protein pellets were resuspended with HU buffer (8 M urea, 5% SDS, 200 mM Tris-HCl pH 6.5, 5 mM EDTA, 0.01% bromophenol blue and 4.5% β-mercaptoethanol). Protein samples were denatured at 65℃ for 10 min and then separated by SDS-PAGE. Vegetive haploid and diploid cells were grown at 30 °C in YPDA medium to OD_{600nm} = 0.4 -0.6. Sporulating cells were first grown at 30 °C for overnight in YPA medium (1% yeast extract, 2% peptone, and 2% potassium acetate or KAc), washed twice with sterilized double distilled water (ddH_2O), transferred into sporulation medium (2% KAc) at zero time point, and harvested at indicated time points. Supplementary Dataset DS10 contains uncropped blots of Figure S1.

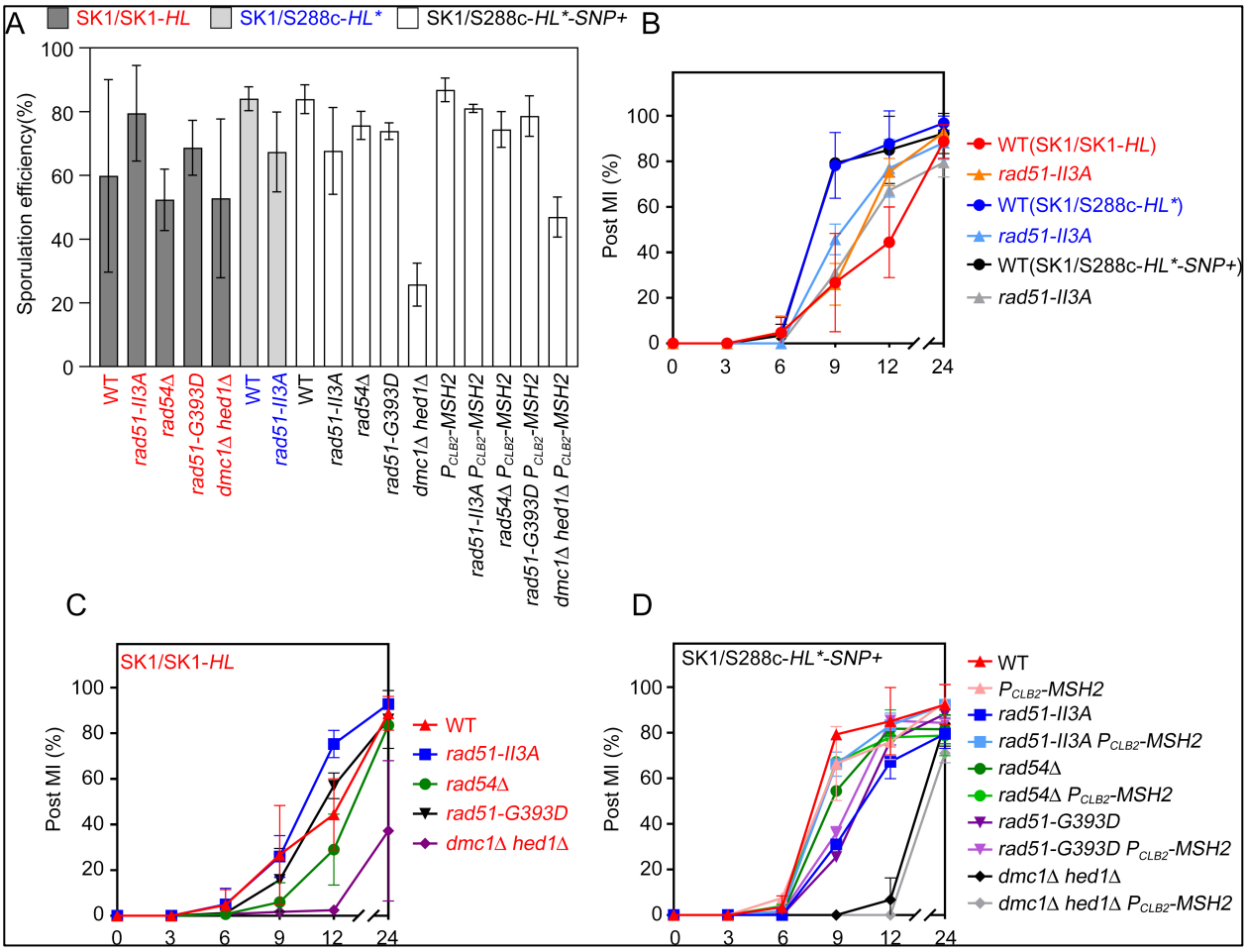

Figure S2. Sporulation efficiency (A) and meiotic progression (B) of the hybrid zygotes analyzed in Figure 1E.

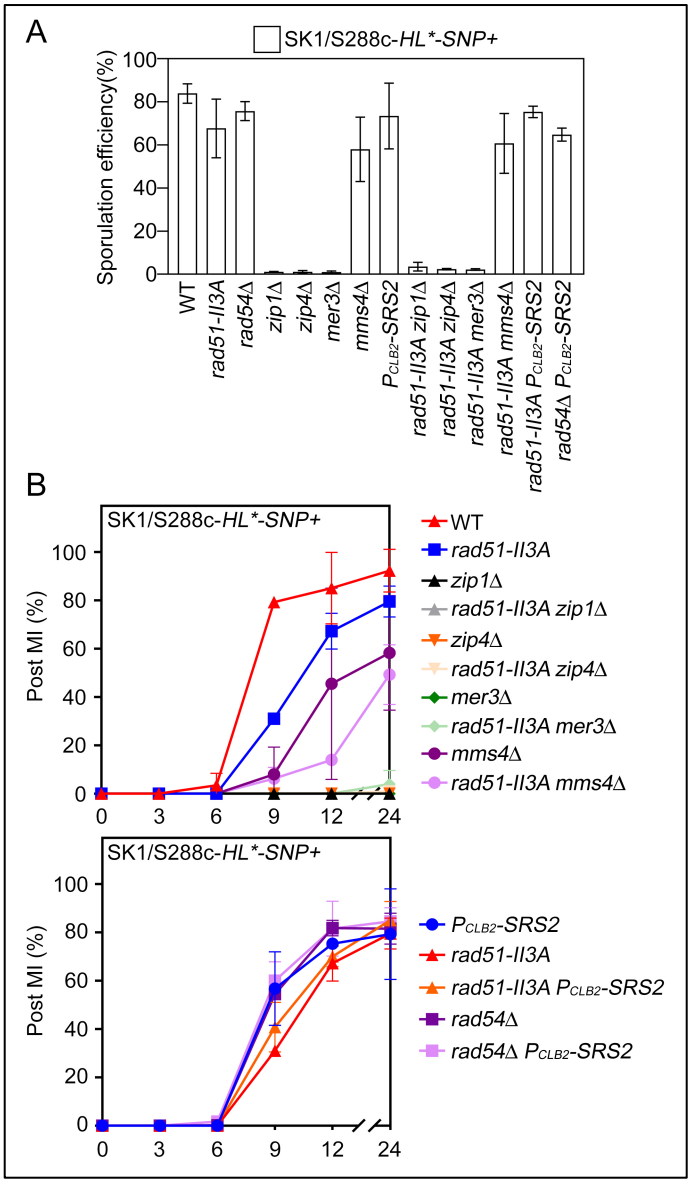

Figure S3. Sporulation efficiency (A) and meiotic progression (B-D) of the hybrid zygotes analyzed in Figure 1F.

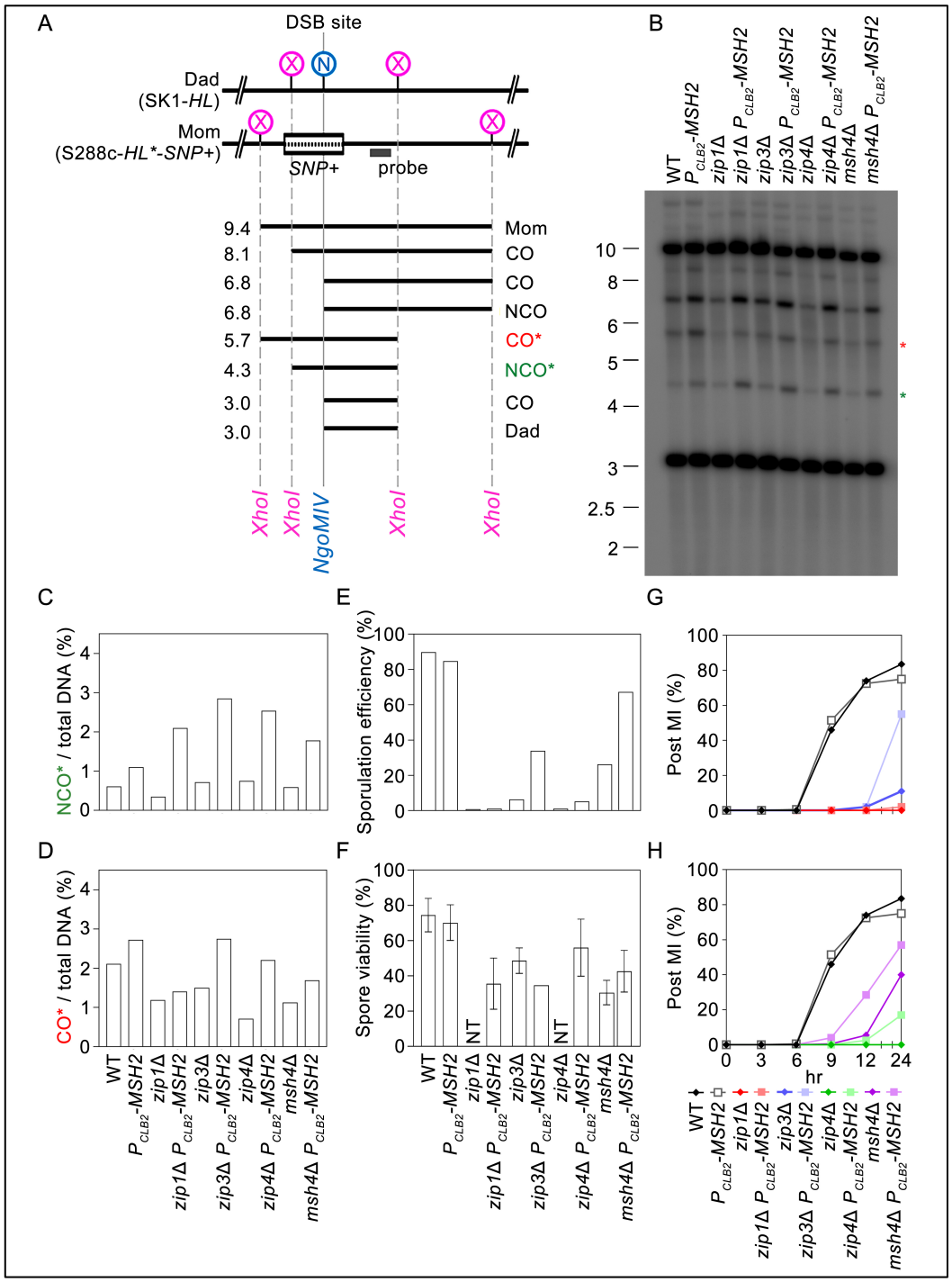

Figure S4. The effect of P_{CLB2}-*MSH2* on the *zmm*Δ SK1/S288c-*HL-*SNP*+ hybrid, including the quantities of recombinants at the *HL**-*SNP*+ DSB hotspot, spore viability, sporulation efficiency, and meiotic progression (see Figure 3).**

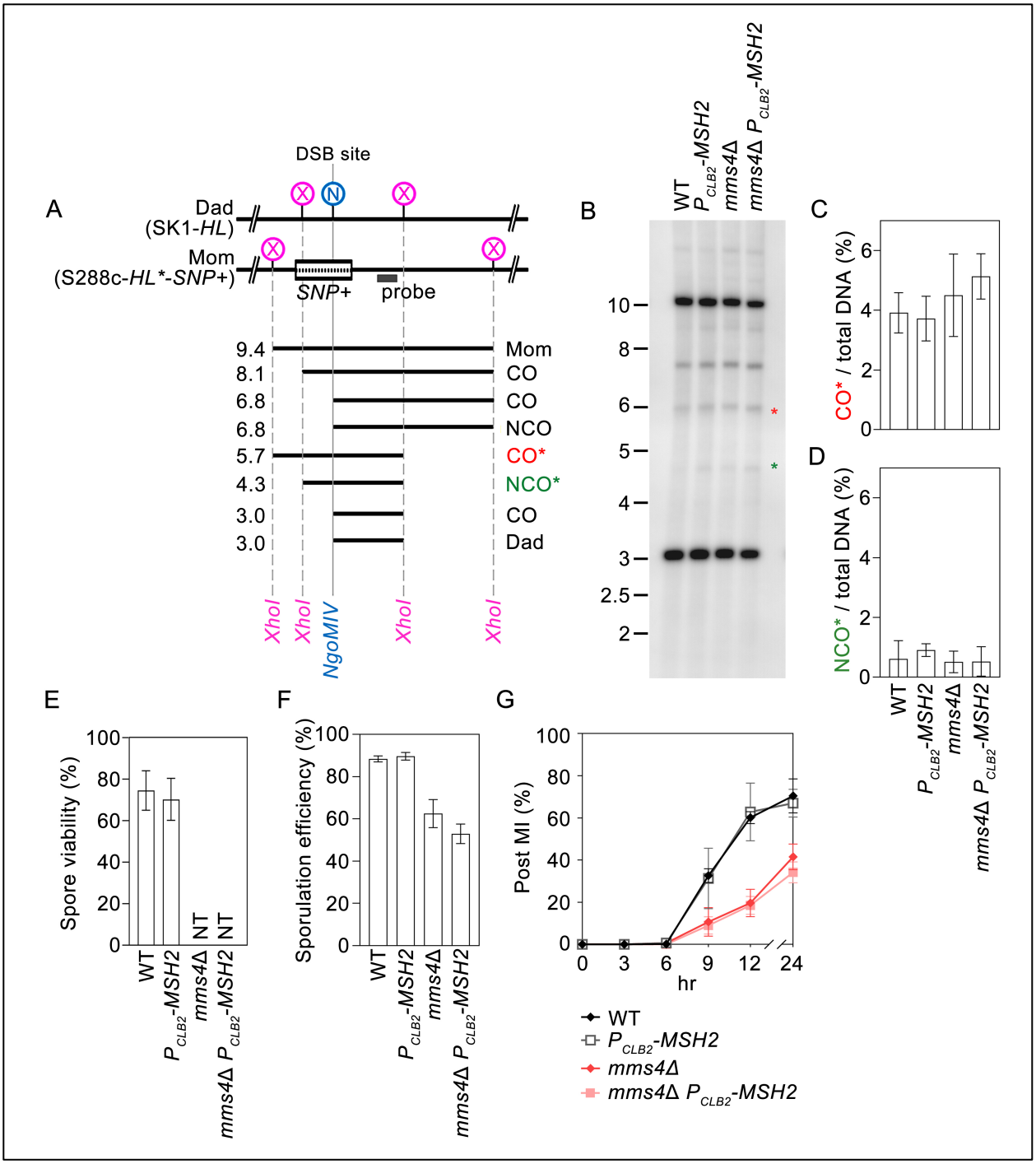

Figure S5. The effect of P_{CLB2}-*MSH2* on the *mms4*Δ SK1/S288c-*HL-*SNP*+ hybrid, including the quantities of recombinants at the *HL**-*SNP*+ DSB hotspot, spore viability, sporulation efficiency, and meiotic progression (see Figure 3).**

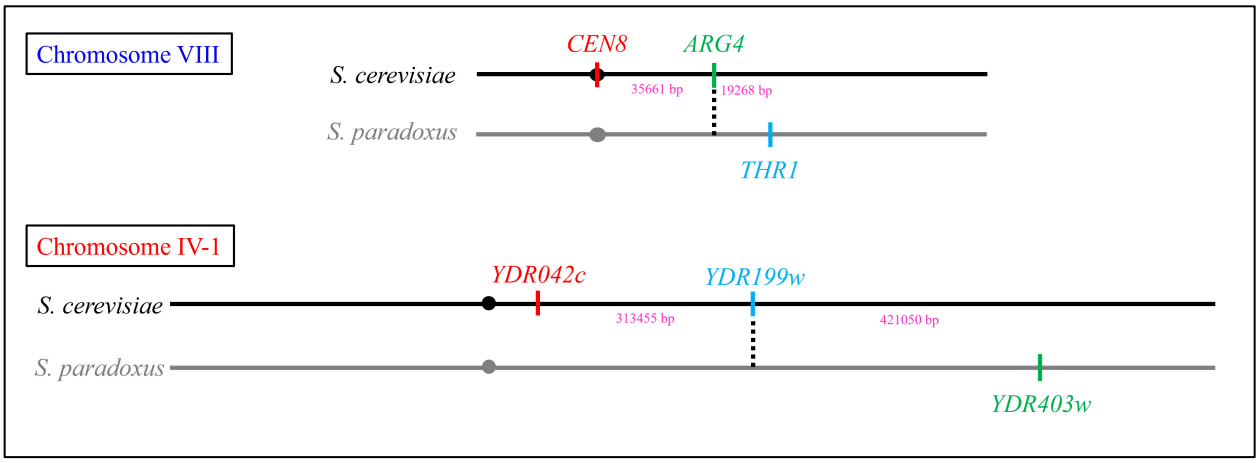

Figure S6. The three interspecies spore-autonomous fluorescent strains used in this study. Illustration of the spore-autonomous fluorescent set-up in N17(*α,VIII, rgC*)/SK1(*a, VIII, RGC*) N17(*a, IV, rcG*)/S288c(*α, IV, RCg*) interspecies hybrid zygotes.

SUPPLEMENTAL INFORMATION

Table S1. List of DNA repair and recombination mutants analyzed in this study.

Dataset DS1. The list of yeast strains, numbers, and genotypes.

Dataset DS2. The raw data of spore viability. All diploid cells were incubated at 30 °C in sporulation medium for at least 24 hours and then scored for their capability to form mature tetrads. Spore viability was determined by isolating the four single spores from each tetrad on YPDA plates.

Dataset DS3. Genome-wide mapping of interhomolog CO and NCO products generated by four wild-type and four rad51-II3A SK1/S288C-*HL**-*SNP*+ hybrid zygotes. The genomic DNA of four representative F1 progeny was determined by PacBio SMRT technology and analyzed by TSETA to identify genome-wide meiotic recombination events as described previously (85,128,130).

Dataset DS4. The distances between two neighboring SNPs and InDels between three indicated genetic intervals (i.e., *CEN8-ARG8-THR1*, *CEN8-ARG8*, and *ARG8-THR1*) of SK1 and N17 near-completed genomic sequences.

Dataset DS5. The spore-autonomous fluorescent raw data of tetrads generated by wild-type and mutant SK1(*a, VIII, rgC*)/SK1(*α, VIII, RGc*) purebred zygotes. Parental ditype (PD), nonparental ditype (NPD), tetratype (T), and MI NDJ tetrads are indicated. The percentages of spores with GFP, CFP and RFP are indicated. Standard errors of genetic distances were calculated using Stahl Laboratory Online Tools (https://elizabethhousworth.com/StahlLabOnlineTools). Interference (γ) is defined as γ = 1 – (coefficient of coincidence or c.o.c.), where c.o.c. is calculated by dividing the actual frequency of double recombinants by the expected frequency (https://en.wikipedia.org/wiki/Coefficient_of_coincidence).

Dataset DS6. The spore-autonomous fluorescent raw data of tetrads generated by wild-type and mutant S288c(*a, VIII, rgC*)/SK1(*α, VIII, RGc*) intraspecies hybrid zygotes.

Dataset DS7. The spore-autonomous fluorescent raw data of tetrads generated by wild-type and mutant N17(*a, VIII, rgC*)/SK1(*α, VIII, RGc*) interspecies hybrid zygotes.

Dataset DS8. The spore-autonomous fluorescent raw data of tetrads generated by wild-type and mutant N17(*a, VIII, rgC*)/SK1(*α, VIII, rgC*) interspecies hybrid zygotes.

Dataset DS9. The spore-autonomous fluorescent raw data of tetrads generated by wild-type N17(*a, IV, rcG*)/S288c(*α, IV, RCg*) interspecies hybrid zygotes.

Dataset DS10. Uncropped immunoblots of Figure S1.

REFERENCES

1. Brown, M.S. and Bishop, D.K. DNA strand exchange and RecA homologs in meiosis. *Cold Spring Harb Perspect Biol*. 2014; 7:a016659.
2. Sasanuma, H., Tawaramoto, M.S., Lao, J.P., Hosaka, H., Sanda, E., Suzuki, M., Yamashita, E., Hunter, N., Shinohara, M., Nakagawa, A. *et al.* A new protein complex promoting the assembly of Rad51 filaments. *Nat Commun*. 2013; 4:1676.
3. Gasior, S.L., Wong, A.K., Kora, Y., Shinohara, A. and Bishop, D.K. Rad52 associates with RPA and functions with Rad55 and Rad57 to assemble meiotic recombination complexes. *Genes Dev*. 1998; 12:2208-2221.
4. Pannunzio, N.R., Manthey, G.M., Liddell, L.C., Fu, B.X., Roberts, C.M. and Bailis, A.M. Rad59 regulates association of Rad52 with DNA double-strand breaks. *Microbiologyopen*. 2012; 1:285-297.
5. Lao, J.P., Oh, S.D., Shinohara, M., Shinohara, A. and Hunter, N. Rad52 promotes postinvasion steps of meiotic double-strand-break repair. *Mol Cell*. 2008; 29:517-524.
6. Nimonkar, A.V., Sica, R.A. and Kowalczykowski, S.C. Rad52 promotes second-end DNA capture in double-stranded break repair to form complement-stabilized joint molecules. *Proc Natl Acad Sci U S A*. 2009; 106:3077-3082.
7. Lan, W.H., Lin, S.Y., Kao, C.Y., Chang, W.H., Yeh, H.Y., Chang, H.Y., Chi, P. and Li, H.W. Rad51 facilitates filament assembly of meiosis-specific Dmc1 recombinase. *Proc Natl Acad Sci U S A*. 2020; 117:11257-11264.
8. Singleton, M.R., Dillingham, M.S. and Wigley, D.B. Structure and mechanism of helicases and nucleic acid translocases. *Annu Rev Biochem*. 2007; 76:23-50.
9. Pyle, A.M. Translocation and unwinding mechanisms of RNA and DNA helicases. *Annu Rev Biophys*. 2008; 37:317-336.
10. Krejci, L., Van Komen, S., Li, Y., Villemain, J., Reddy, M.S., Klein, H., Ellenberger, T. and Sung, P. DNA helicase Srs2 disrupts the Rad51 presynaptic filament. *Nature*. 2003; 423:305-309.
11. Veaute, X., Jeusset, J., Soustelle, C., Kowalczykowski, S.C., Le Cam, E. and Fabre, F. The Srs2 helicase prevents recombination by disrupting Rad51 nucleoprotein filaments. *Nature*. 2003; 423:309-312.
12. Liu, J., Renault, L., Veaute, X., Fabre, F., Stahlberg, H. and Heyer, W.D. Rad51 paralogues Rad55-Rad57 balance the antirecombinase Srs2 in Rad51 filament formation. *Nature*. 2011; 479:245-248.
13. Sasanuma, H., Furihata, Y., Shinohara, M. and Shinohara, A. Remodeling of the Rad51 DNA strand-exchange protein by the Srs2 helicase. *Genetics*. 2013; 194:859-872.
14. Crickard, J.B., Kaniecki, K., Kwon, Y., Sung, P. and Greene, E.C. Meiosis-specific recombinase Dmc1 is a potent inhibitor of the Srs2 antirecombinase. *Proc Natl Acad Sci U S A*. 2018; 115:E10041-E10048.
15. Nimonkar, A.V., Dombrowski, C.C., Siino, J.S., Stasiak, A.Z., Stasiak, A. and Kowalczykowski, S.C. *Saccharomyces cerevisiae* Dmc1 and Rad51 proteins preferentially function with Tid1 and Rad54 proteins, respectively, to promote DNA strand invasion during genetic recombination. *J Biol Chem*. 2012; 287:28727-28737.
16. Meir, A., Crickard, J.B., Kwon, Y., Sung, P. and Greene, E.C. Rad54 and Rdh54 prevent Srs2-mediated disruption of Rad51 presynaptic filaments. *Proc Natl Acad Sci U S A*. 2022; 119.

17. Tsubouchi, H. and Roeder, G.S. Budding yeast Hed1 down-regulates the mitotic recombination machinery when meiotic recombination is impaired. *Genes Dev*. 2006; 20:1766-1775.
18. Busygina, V., Sehorn, M.G., Shi, I.Y., Tsubouchi, H., Roeder, G.S. and Sung, P. Hed1 regulates Rad51-mediated recombination via a novel mechanism. *Genes Dev*. 2008; 22:786-795.
19. Ziesel, A., Weng, Q., Ahuja, J.S., Bhattacharya, A., Dutta, R., Cheng, E., Borner, G.V., Lichten, M. and Hollingsworth, N.M. Rad51-mediated interhomolog recombination during budding yeast meiosis is promoted by the meiotic recombination checkpoint and the conserved Pif1 helicase. *PLoS Genet*. 2022; 18:e1010407.
20. De Muyt, A., Jessop, L., Kolar, E., Sourirajan, A., Chen, J., Dayani, Y. and Lichten, M. BLM helicase ortholog Sgs1 is a central regulator of meiotic recombination intermediate metabolism. *Mol Cell*. 2012; 46:43-53.
21. Sandhu, R., Monge Neria, F., Monge Neria, J., Chen, X., Hollingsworth, N.M. and Borner, G.V. DNA helicase Mph1(FANCM) ensures meiotic recombination between parental chromosomes by dissociating precocious displacement loops. *Dev Cell*. 2020; 53:458-472 e455.
22. Allers, T. and Lichten, M. Differential timing and control of noncrossover and crossover recombination during meiosis. *Cell*. 2001; 106:47-57.
23. Hunter, N. and Kleckner, N. The single-end invasion: an asymmetric intermediate at the double-strand break to double-holliday junction transition of meiotic recombination. *Cell*. 2001; 106:59-70.
24. Borner, G.V., Kleckner, N. and Hunter, N. Crossover/noncrossover differentiation, synaptonemal complex formation, and regulatory surveillance at the leptotene/zygotene transition of meiosis. *Cell*. 2004; 117:29-45.
25. Hunter, N. Meiotic recombination: The essence of heredity. *Cold Spring Harb Perspect Biol*. 2015; 7.
26. Ahuja, J.S., Harvey, C.S., Wheeler, D.L. and Lichten, M. Repeated strand invasion and extensive branch migration are hallmarks of meiotic recombination. *Mol Cell*. 2021; 81:4258-4270 e4254.
27. Matson, S.W. and Robertson, A.B. The UvrD helicase and its modulation by the mismatch repair protein MutL. *Nucleic Acids Res*. 2006; 34:4089-4097.
28. Kolodner, R.D. and Marsischky, G.T. Eukaryotic DNA mismatch repair. *Curr Opin Genet Dev*. 1999; 9:89-96.
29. Smith, C.E., Bowen, N., Graham, W.J.t., Goellner, E.M., Srivatsan, A. and Kolodner, R.D. Activation of Saccharomyces cerevisiae Mlh1-Pms1 Endonuclease in a Reconstituted Mismatch Repair System. *J Biol Chem*. 2015; 290:21580-21590.
30. Wang, T.F., Kleckner, N. and Hunter, N. Functional specificity of MutL homologs in yeast: evidence for three Mlh1-based heterocomplexes with distinct roles during meiosis in recombination and mismatch correction. *Proc Natl Acad Sci U S A*. 1999; 96:13914-13919.
31. Campbell, C.S., Hombauer, H., Srivatsan, A., Bowen, N., Gries, K., Desai, A., Putnam, C.D. and Kolodner, R.D. Mlh2 is an accessory factor for DNA mismatch repair in Saccharomyces cerevisiae. *PLoS Genet*. 2014; 10:e1004327.
32. Sugawara, N., Goldfarb, T., Studamire, B., Alani, E. and Haber, J.E. Heteroduplex rejection during single-strand annealing requires Sgs1 helicase and mismatch repair proteins Msh2 and Msh6 but not Pms1. *Proc Natl Acad Sci U S A*. 2004; 101:9315-9320.

33. Duroc, Y., Kumar, R., Ranjha, L., Adam, C., Guerois, R., Md Muntaz, K., Marsolier-Kergoat, M.C., Dingli, F., Laureau, R., Loew, D. *et al.* Concerted action of the MutLbeta heterodimer and Mer3 helicase regulates the global extent of meiotic gene conversion. *Elife*. 2017; 6.
34. Altmannova, V., Firlej, M., Muller, F., Janning, P., Rauleder, R., Rousova, D., Schaffler, A., Bange, T. and Weir, J.R. Biochemical characterisation of Mer3 helicase interactions and the protection of meiotic recombination intermediates. *Nucleic Acids Res*. 2023.
35. Hunter, N. and Borts, R.H. Mlh1 is unique among mismatch repair proteins in its ability to promote crossing-over during meiosis. *Genes Dev*. 1997; 11:1573-1582.
36. Buchhop, S., Gibson, M.K., Wang, X.W., Wagner, P., Sturzbecher, H.W. and Harris, C.C. Interaction of p53 with the human Rad51 protein. *Nucleic Acids Res*. 1997; 25:3868-3874.
37. Abdullah, M.F., Hoffmann, E.R., Cotton, V.E. and Borts, R.H. A role for the MutL homologue MLH2 in controlling heteroduplex formation and in regulating between two different crossover pathways in budding yeast. *Cytogenet Genome Res*. 2004; 107:180-190.
38. Zakharyevich, K., Tang, S., Ma, Y. and Hunter, N. Delineation of joint molecule resolution pathways in meiosis identifies a crossover-specific resolvase. *Cell*. 2012; 149:334-347.
39. Rogacheva, M.V., Manhart, C.M., Chen, C., Guarne, A., Surtees, J. and Alani, E. Mlh1-Mlh3, a meiotic crossover and DNA mismatch repair factor, is a Msh2-Msh3-stimulated endonuclease. *J Biol Chem*. 2014; 289:5664-5673.
40. Cannavo, E., Sanchez, A., Anand, R., Ranjha, L., Hugener, J., Adam, C., Acharya, A., Weyland, N., Aran-Guiu, X., Charbonnier, J.B. *et al.* Regulation of the MLH1-MLH3 endonuclease in meiosis. *Nature*. 2020; 586:618-622.
41. Veaute, X., Delmas, S., Selva, M., Jeusset, J., Le Cam, E., Matic, I., Fabre, F. and Petit, M.A. UvrD helicase, unlike Rep helicase, dismantles RecA nucleoprotein filaments in *Escherichia coli*. *EMBO J*. 2005; 24:180-189.
42. Meir, A., Raina, V.B., Rivera, C.E., Marie, L., Symington, L.S. and Greene, E.C. The separation pin distinguishes the pro- and anti-recombinogenic functions of *Saccharomyces cerevisiae* Srs2. *Nat Commun*. 2023; 14:8144.
43. Griffiths, A., Doebley, j. and Peichel, C. (2008) *Introduction to Genetic Analysis*. W. H. Freeman and Company, New York.
44. Berchowitz, L.E. and Copenhaver, G.P. Genetic interference: Don't stand so close to me. *Current Genomics*. 2010; 11:91-102.
45. Zhang, L., Liang, Z., Hutchinson, J. and Kleckner, N. Crossover patterning by the beam-film model: analysis and implications. *PLoS Genet*. 2014; 10:e1004042.
46. Chuang, Y.C. and Smith, G.R. Meiotic crossover interference: Methods of analysis and mechanisms of action. *Curr Top Dev Biol*. 2023; 151:217-244.
47. Lynn, A., Soucek, R. and Borner, G.V. ZMM proteins during meiosis: crossover artists at work. *Chromosome Res*. 2007; 15:591-605.
48. de los Santos, T., Hunter, N., Lee, C., Larkin, B., Loidl, J. and Hollingsworth, N.M. The Mus81/Mms4 endonuclease acts independently of double-Holliday junction resolution to promote a distinct subset of crossovers during meiosis in budding yeast. *Genetics*. 2003; 164:81-94.
49. Shinohara, M., Oh, S.D., Hunter, N. and Shinohara, A. Crossover assurance and crossover interference are distinctly regulated by the ZMM proteins during yeast meiosis. *Nat Genet*. 2008; 40:299-309.

50. Girard, C., Zwicker, D. and Mercier, R. The regulation of meiotic crossover distribution: a coarse solution to a century-old mystery? *Biochem Soc Trans*. 2023; 51:1179-1190.
51. White, M.A., Weiner, B., Chu, L., Lim, G. and Kleckner, N.E. Crossover interference mediates multiscale patterning along meiotic chromosomes. *bioRxiv*. 2024.
52. Svendsen, J.M. and Harper, J.W. GEN1/Yen1 and the SLX4 complex: Solutions to the problem of Holliday junction resolution. *Genes Dev*. 2010; 24:521-536.
53. Schwartz, E.K. and Heyer, W.D. Processing of joint molecule intermediates by structure-selective endonucleases during homologous recombination in eukaryotes. *Chromosoma*. 2011; 120:109-127.
54. Saponaro, M., Callahan, D., Zheng, X., Krejci, L., Haber, J.E., Klein, H.L. and Liberi, G. Cdk1 targets Srs2 to complete synthesis-dependent strand annealing and to promote recombinational repair. *PLoS Genet*. 2010; 6:e1000858.
55. Miura, T., Shibata, T. and Kusano, K. Putative antirecombinase Srs2 DNA helicase promotes noncrossover homologous recombination avoiding loss of heterozygosity. *Proc Natl Acad Sci U S A*. 2013; 110:16067-16072.
56. Chavdarova, M., Marini, V., Sisakova, A., Sedlackova, H., Vigasova, D., Brill, S.J., Lisby, M. and Krejci, L. Srs2 promotes Mus81-Mms4-mediated resolution of recombination intermediates. *Nucleic Acids Res*. 2015; 43:3626-3642.
57. Liu, J., Ede, C., Wright, W.D., Gore, S.K., Jenkins, S.S., Freudenthal, B.D., Todd Washington, M., Veaute, X. and Heyer, W.D. Srs2 promotes synthesis-dependent strand annealing by disrupting DNA polymerase delta-extending D-loops. *Elife*. 2017; 6.
58. Oh, S.D., Lao, J.P., Taylor, A.F., Smith, G.R. and Hunter, N. RecQ helicase, Sgs1, and XPF family endonuclease, Mus81-Mms4, resolve aberrant joint molecules during meiotic recombination. *Mol Cell*. 2008; 31:324-336.
59. Oh, S.D., Jessop, L., Lao, J.P., Allers, T., Lichten, M. and Hunter, N. Stabilization and electrophoretic analysis of meiotic recombination intermediates in *Saccharomyces cerevisiae*. *Methods Mol Biol*. 2009; 557:209-234.
60. Lukaszewicz, A., Howard-Till, R.A. and Loidl, J. Mus81 nuclease and Sgs1 helicase are essential for meiotic recombination in a protist lacking a synaptonemal complex. *Nucleic Acids Res*. 2013; 41:9296-9309.
61. Rockmill, B., Fung, J.C., Branda, S.S. and Roeder, G.S. The Sgs1 helicase regulates chromosome synapsis and meiotic crossing over. *Curr Biol*. 2003; 13:1954-1962.
62. Jessop, L., Rockmill, B., Roeder, G.S. and Lichten, M. Meiotic chromosome synapsis-promoting proteins antagonize the anti-crossover activity of sgs1. *PLoS Genet*. 2006; 2:e155.
63. Oh, S.D., Lao, J.P., Hwang, P.Y., Taylor, A.F., Smith, G.R. and Hunter, N. BLM ortholog, Sgs1, prevents aberrant crossing-over by suppressing formation of multichromatid joint molecules. *Cell*. 2007; 130:259-272.
64. Jessop, L. and Lichten, M. Mus81/Mms4 endonuclease and Sgs1 helicase collaborate to ensure proper recombination intermediate metabolism during meiosis. *Mol Cell*. 2008; 31:313-323.
65. Klein, H.L. and Symington, L.S. Sgs1--the maestro of recombination. *Cell*. 2012; 149:257-259.
66. Borts, R.H., Lichten, M., Hearn, M., Davidow, L.S. and Haber, J.E. Physical monitoring of meiotic recombination in *Saccharomyces cerevisiae*. *Cold Spring Harb Symp Quant Biol*. 1984; 49:67-76.

67. Borts, R.H., Lichten, M. and Haber, J.E. Analysis of meiosis-defective mutations in yeast by physical monitoring of recombination. *Genetics*. 1986; 113:551-567.
68. Lichten, M., Borts, R.H. and Haber, J.E. Meiotic gene conversion and crossing over between dispersed homologous sequences occurs frequently in *Saccharomyces cerevisiae*. *Genetics*. 1987; 115:233-246.
69. Rayssiguier, C., Thaler, D.S. and Radman, M. The barrier to recombination between *Escherichia coli* and *Salmonella typhimurium* is disrupted in mismatch-repair mutants. *Nature*. 1989; 342:396-401.
70. Cohan, F.M. Genetic exchange and evolutionary divergence in prokaryotes. *Trends Ecol Evol*. 1994; 9:175-180.
71. Hunter, N., Chambers, S.R., Louis, E.J. and Borts, R.H. The mismatch repair system contributes to meiotic sterility in an interspecific yeast hybrid. *EMBO J*. 1996; 15:1726-1733.
72. Datta, A., Adjiri, A., New, L., Crouse, G.F. and Jinks Robertson, S. Mitotic crossovers between diverged sequences are regulated by mismatch repair proteins in Saccaromyces cerevisiae. *Mol Cell Biol*. 1996; 16:1085-1093.
73. Majewski, J. and Cohan, F.M. The effect of mismatch repair and heteroduplex formation on sexual isolation in Bacillus. *Genetics*. 1998; 148:13-18.
74. Sniegowski, P. Mismatch repair: origin of species? *Curr Biol*. 1998; 8:R59-61.
75. Myung, K., Datta, A., Chen, C. and Kolodner, R.D. *SGS1*, the *Saccharomyces cerevisiae* homologue of BLM and WRN, suppresses genome instability and homeologous recombination. *Nat Genet*. 2001; 27:113-116.
76. Greig, D., Travisano, M., Louis, E.J. and Borts, R.H. A role for the mismatch repair system during incipient speciation in *Saccharomyces*. *J Evol Biol*. 2003; 16:429-437.
77. Coyne, J.A. and O'rr, H.A. (2004) *Speciation*. Sinauer Associates, Sunderland, MA.
78. Liti, G., Barton, D.B. and Louis, E.J. Sequence diversity, reproductive isolation and species concepts in *Saccharomyces*. *Genetics*. 2006; 174:839-850.
79. Spies, M. and Fishel, R. Mismatch repair during homologous and homeologous recombination. *Cold Spring Harb Perspect Biol*. 2015; 7:a022657.
80. Chakraborty, U. and Alani, E. Understanding how mismatch repair proteins participate in the repair/anti-recombination decision. *FEMS Yeast Res*. 2016; 16.
81. Martini, E., Borde, V., Legendre, M., Audic, S., Regnault, B., Soubigou, G., Dujon, B. and Llorente, B. Genome-wide analysis of heteroduplex DNA in mismatch repair-deficient yeast cells reveals novel properties of meiotic recombination pathways. *PLoS Genet*. 2011; 7:e1002305.
82. Bozdag, G.O., Ono, J., Denton, J.A., Karakoc, E., Hunter, N., Leu, J.Y. and Greig, D. Breaking a species barrier by enabling hybrid recombination. *Curr Biol*. 2021; 31:R180-R181.
83. Lee, B.H. and Amon, A. Role of Polo-like kinase *CDC5* in programming meiosis I chromosome segregation. *Science*. 2003; 300:482-486.
84. Spell, R.M. and Jinks-Robertson, S. Examination of the roles of Sgs1 and Srs2 helicases in the enforcement of recombination fidelity in *Saccharomyces cerevisiae*. *Genetics*. 2004; 168:1855-1865.
85. Li, W.C., Lee, C.Y., Lan, W.H., Woo, T.T., Liu, H.C., Yeh, H.Y., Chang, H.Y., Chuang, Y.C., Chen, C.Y., Chuang, C.N. *et al. Trichoderma reesei* Rad51 tolerates mismatches in

hybrid meiosis with diverse genome sequences. *Proc Natl Acad Sci*. 2021; 118:e2007192118.
86. Joshi, N., Brown, M.S., Bishop, D.K. and Borner, G.V. Gradual implementation of the meiotic recombination program via checkpoint pathways controlled by global DSB levels. *Mol Cell*. 2015; 57:797-811.
87. Xu, L., Weiner, B.M. and Kleckner, N. Meiotic cells monitor the status of the interhomolog recombination complex. *Genes Dev*. 1997; 11:106-118.
88. He, W., Rao, H., Tang, S., Bhagwat, N., Kulkarni, D.S., Ma, Y., Chang, M.A.W., Hall, C., Bragg, J.W., Manasca, H.S. *et al.* Regulated proteolysis of MutSgamma controls meiotic crossing over. *Mol Cell*. 2020; 78:168-183 e165.
89. Schmuckli-Maurer, J. and Heyer, W.D. Meiotic recombination in *RAD54* mutants of *Saccharomyces cerevisiae*. *Chromosoma*. 2000; 109:86-93.
90. Callender, T.L., Laureau, R., Wan, L., Chen, X., Sandhu, R., Laljee, S., Zhou, S., Suhandynata, R.T., Prugar, E., Gaines, W.A. *et al.* Mek1 down regulates Rad51 activity during yeast meiosis by phosphorylation of Hed1. *PLoS Genet*. 2016; 12:e1006226.
91. Cloud, V., Chan, Y.L., Grubb, J., Budke, B. and Bishop, D.K. Rad51 is an accessory factor for Dmc1-mediated joint molecule formation during meiosis. *Science*. 2012; 337:1222-1225.
92. Woo, T.T., Chuang, C.N., Higashide, M., Shinohara, A. and Wang, T.F. Dual roles of yeast Rad51 N-terminal domain in repairing DNA double-strand breaks. *Nucleic Acids Res*. 2020; 48:8474-8489.
93. Bertuch, A.A. and Lundblad, V. Which end: dissecting Ku's function at telomeres and double-strand breaks. *Genes Dev*. 2003; 17:2347-2350.
94. Mazina, O.M., Mazin, A.V., Nakagawa, T., Kolodner, R.D. and Kowalczykowski, S.C. Saccharomyces cerevisiae Mer3 helicase stimulates 3'-5' heteroduplex extension by Rad51; implications for crossover control in meiotic recombination. *Cell*. 2004; 117:47-56.
95. Vernekar, D.V., Reginato, G., Adam, C., Ranjha, L., Dingli, F., Marsolier, M.C., Loew, D., Guerois, R., Llorente, B., Cejka, P. *et al.* The Pif1 helicase is actively inhibited during meiotic recombination which restrains gene conversion tract length. *Nucleic Acids Res*. 2021; 49:4522-4533.
96. Seong, C., Colavito, S., Kwon, Y., Sung, P. and Krejci, L. Regulation of Rad51 recombinase presynaptic filament assembly via interactions with the Rad52 mediator and the Srs2 anti-recombinase. *J Biol Chem*. 2009; 284:24363-24371.
97. Davis, A.P. and Symington, L.S. The yeast recombinational repair protein Rad59 interacts with Rad52 and stimulates single-strand annealing. *Genetics*. 2001; 159:515-525.
98. Sym, M., Engebrecht, J.A. and Roeder, G.S. Zip1 is a synaptonemal complex protein required for meiotic chromosome synapsis. *Cell*. 1993; 72:365-378.
99. Humphryes, N., Leung, W.K., Argunhan, B., Terentyev, Y., Dvorackova, M. and Tsubouchi, H. The Ecm11-Gmc2 complex promotes synaptonemal complex formation through assembly of transverse filaments in budding yeast. *PLoS Genet*. 2013; 9:e1003194.
100. Pyatnitskaya, A., Andreani, J., Guerois, R., De Muyt, A. and Borde, V. The Zip4 protein directly couples meiotic crossover formation to synaptonemal complex assembly. *Genes Dev*. 2022; 36:53-69.
101. De Muyt, A., Pyatnitskaya, A., Andreani, J., Ranjha, L., Ramus, C., Laureau, R., Fernandez-Vega, A., Holoch, D., Girard, E., Govin, J. *et al.* A meiotic XPF-ERCC1-like

complex recognizes joint molecule recombination intermediates to promote crossover formation. *Genes Dev*. 2018; 32:283-296.
102. Ross-Macdonald, P. and Roeder, G.S. Mutation of a meiosis-specific MutS homolog decreases crossing over but not mismatch correction. *Cell*. 1994; 79:1069-1080.
103. Hollingsworth, N.M., Ponte, L. and Halsey, C. *MSH5*, a novel MutS homolog, facilitates meiotic reciprocal recombination between homologs in *Saccharomyces cerevisiae* but not mismatch repair. *Genes Dev*. 1995; 9:1728-1739.
104. Ahuja, J.S., Sandhu, R., Mainpal, R., Lawson, C., Henley, H., Hunt, P.A., Yanowitz, J.L. and Borner, G.V. Control of meiotic pairing and recombination by chromosomally tethered 26S proteasome. *Science*. 2017; 355:408-411.
105. Agarwal, S. and Roeder, G.S. Zip3 provides a link between recombination enzymes and synaptonemal complex proteins. *Cell*. 2000; 102:245-255.
106. Perry, J., Kleckner, N. and Borner, G.V. Bioinformatic analyses implicate the collaborating meiotic crossover/chiasma proteins Zip2, Zip3, and Spo22/Zip4 in ubiquitin labeling. *Proc Natl Acad Sci U S A*. 2005; 102:17594-17599.
107. Cheng, C.H., Lo, Y.H., Liang, S.S., Ti, S.C., Lin, F.M., Yeh, C.H., Huang, H.Y. and Wang, T.F. SUMO modifications control assembly of synaptonemal complex and polycomplex in meiosis of *Saccharomyces cerevisiae*. *Genes Dev*. 2006; 20:2067-2081.
108. Reynolds, A., Qiao, H., Yang, Y., Chen, J.K., Jackson, N., Biswas, K., Holloway, J.K., Baudat, F., de Massy, B., Wang, J. *et al.* RNF212 is a dosage-sensitive regulator of crossing-over during mammalian meiosis. *Nat Genet*. 2013; 45:269-278.
109. Qiao, H., Prasada Rao, H.B., Yang, Y., Fong, J.H., Cloutier, J.M., Deacon, D.C., Nagel, K.E., Swartz, R.K., Strong, E., Holloway, J.K. *et al.* Antagonistic roles of ubiquitin ligase HEI10 and SUMO ligase RNF212 regulate meiotic recombination. *Nat Genet*. 2014; 46:194-199.
110. Fung, J.C., Rockmill, B., Odell, M. and Roeder, G.S. Imposition of crossover interference through the nonrandom distribution of synapsis initiation complexes. *Cell*. 2004; 116:795-802.
111. Thacker, D., Lam, I., Knop, M. and Keeney, S. Exploiting spore-autonomous fluorescent protein expression to quantify meiotic chromosome behaviors in *Saccharomyces cerevisiae*. *Genetics*. 2011; 189:423-439.
112. Petukhova, G., Stratton, S. and Sung, P. Catalysis of homologous DNA pairing by yeast Rad51 and Rad54 proteins. *Nature*. 1998; 393:91-94.
113. Petukhova, G., Van Komen, S., Vergano, S., Klein, H. and Sung, P. Yeast Rad54 promotes Rad51-dependent homologous DNA pairing via ATP hydrolysis-driven change in DNA double helix conformation. *J Biol Chem*. 1999; 274:29453-29462.
114. Choi, J., Kong, M., Gallagher, D.N., Li, K., Bronk, G., Cao, Y., Greene, E.C. and Haber, J.E. Repair of mismatched templates during Rad51-dependent Break-Induced Replication. *PLoS Genet*. 2022; 18:e1010056.
115. Lee, J.Y., Terakawa, T., Qi, Z., Steinfeld, J.B., Redding, S., Kwon, Y., Gaines, W.A., Zhao, W., Sung, P. and Greene, E.C. DNA recombination. Base triplet stepping by the Rad51/RecA family of recombinases. *Science*. 2015; 349:977-981.
116. Qi, Z., Redding, S., Lee, J.Y., Gibb, B., Kwon, Y., Niu, H., Gaines, W.A., Sung, P. and Greene, E.C. DNA sequence alignment by microhomology sampling during homologous recombination. *Cell*. 2015; 160:856-869.

117. Borgogno, M.V., Monti, M.R., Zhao, W., Sung, P., Argarana, C.E. and Pezza, R.J. Tolerance of DNA mismatches in Dmc1 recombinase-mediated DNA strand exchange. *J Biol Chem*. 2016; 291:4928-4938.
118. Lee, J.Y., Steinfeld, J.B., Qi, Z., Kwon, Y., Sung, P. and Greene, E.C. Sequence imperfections and base triplet recognition by the Rad51/RecA family of recombinases. *J Biol Chem*. 2017; 292:11125-11135.
119. Luo, S.C., Yeh, H.Y., Lan, W.H., Wu, Y.M., Yang, C.H., Chang, H.Y., Su, G.C., Lee, C.Y., Wu, W.J., Li, H.W. *et al.* Identification of fidelity-governing factors in human recombinases DMC1 and RAD51 from cryo-EM structures. *Nat Commun*. 2021; 12:115.
120. Xu, J., Zhao, L., Peng, S., Chu, H., Liang, R., Tian, M., Connell, P.P., Li, G., Chen, C. and Wang, H.W. Mechanisms of distinctive mismatch tolerance between Rad51 and Dmc1 in homologous recombination. *Nucleic Acids Res*. 2021.
121. Sirr, A., Timour, M.S., Cromie, G.A., Tang, M. and Dudley, A.M. A method for quantifying sporulation efficiency and isolating meiotic progeny in non-GMO strains of *Saccharomyces cerevisiae*. *Yeast*. 2022; 39:354-362.
122. Alani, E., Padmore, R. and Kleckner, N. Analysis of wild-type and *rad50* mutants of yeast suggests an intimate relationship between meiotic chromosome synapsis and recombination. *Cell*. 1990; 61:419-436.
123. Padmore, R., Cao, L. and Kleckner, N. Temporal comparison of recombination and synaptonemal complex formation during meiosis in *S. cerevisiae*. *Cell*. 1991; 66:1239-1256.
124. Niu, H., Wan, L., Busygina, V., Kwon, Y., Allen, J.A., Li, X., Kunz, R.C., Kubota, K., Wang, B., Sung, P. *et al.* Regulation of meiotic recombination via Mek1-mediated Rad54 phosphorylation. *Mol Cell*. 2009; 36:393-404.
125. Jovanska, L., Lin, I.C., Yao, J.S., Chen, C.L., Liu, H.C., Li, W.C., Chuang, Y.C., Chuang, C.N., Yu, A.C., Lin, H.N. *et al.* DNA cytosine methyltransferases differentially regulate genome-wide hypermutation and interhomolog recombination in *Trichoderma reesei* meiosis. *Nucleic Acids Res*. 2024; 52:9551-9573.
126. Zickler, D. and Kleckner, N. Recombination, pairing, and synapsis of homologs during meiosis. *Cold Spring Harb Perspect Biol*. 2015; 7.
127. von Diezmann, L. and Rog, O. Let's get physical - mechanisms of crossover interference. *J Cell Sci*. 2021; 134.
128. Li, W.C., Liu, H.C., Lin, Y.J., Tung, S.Y. and Wang, T.F. Third-generation sequencing-based mapping and visualization of single nucleotide polymorphism, meiotic recombination, illegitimate mutation and repeat-induced point mutation *NAR Genomics and Bioinformatics*. 2020; 2:lqaa056.
129. Li, W.C. and Wang, T.F. PacBio long-read sequencing, assembly, and funannotate reannotation of the complete genome of *Trichoderma reesei* QM6a. *Methods Mol Biol*. 2021; 2234:311-329.
130. Liu, H.C., Li, W.C. and Wang, T.F. TSETA: A third-generation sequencing-based computational tool for mapping and visualization of SNPs, meiotic recombination products, and RIP mutations. *Methods Mol Biol*. 2021; 2234:331-361.
131. Chen, C.L., Li, W.C., Chuang, Y.C., Liu, H.C., Huang, C.H., Lo, K.Y., Chen, C.Y., Chang, F.M., Chang, G.A., Lin, Y.L. *et al.* Sexual crossing, chromosome-Level genome sequences, and comparative genomic analyses for the medicinal mushroom *Taiwanofungus*

Camphoratus (Syn. *Antrodia Cinnamomea*, *Antrodia Camphorata*). *Microbiol Spectr*. 2022; 10:e0203221.
132. De La Cerda, G.Y., Landis, J.B., Eifler, E., Hernandez, A.I., Li, F.W., Zhang, J., Tribble, C.M., Karimi, N., Chan, P., Givnish, T. *et al.* Balancing read length and sequencing depth: Optimizing Nanopore long-read sequencing for monocots with an emphasis on the Liliales. *Appl Plant Sci*. 2023; 11:e11524.
133. Anderson, L.K., Reeves, A., Webb, L.M. and Ashley, T. Distribution of crossing over on mouse synaptonemal complexes using immunofluorescent localization of MLH1 protein. *Genetics*. 1999; 151:1569-1579.
134. Chelysheva, L., Grandont, L., Vrielynck, N., le Guin, S., Mercier, R. and Grelon, M. An easy protocol for studying chromatin and recombination protein dynamics during *Arabidopsis thaliana* meiosis: immunodetection of cohesins, histones and MLH1. *Cytogenet Genome Res*. 2010; 129:143-153.
135. Yokoo, R., Zawadzki, K.A., Nabeshima, K., Drake, M., Arur, S. and Villeneuve, A.M. COSA-1 reveals robust homeostasis and separable licensing and reinforcement steps governing meiotic crossovers. *Cell*. 2012; 149:75-87.
136. Yue, J.X., Li, J., Aigrain, L., Hallin, J., Persson, K., Oliver, K., Bergstrom, A., Coupland, P., Warringer, J., Lagomarsino, M.C. *et al.* Contrasting evolutionary genome dynamics between domesticated and wild yeasts. *Nat Genet*. 2017; 49:913-924.
137. Stahl, F.W. and Housworth, E.A. Methods for analysis of crossover interference in *Saccharomyces cerevisiae*. *Methods Mol Biol*. 2009; 557:35-53.
138. Snow, R. Maximum likelihood estimation of linkage and interference from tetrad data. *Genetics*. 1979; 92:231-245.
139. Stahl, F.W. On the "NPD ratio" as a test for crossover interference. *Genetics*. 2008; 179:701-704.
140. Dluzewska, J., Dziegielewski, W., Szymanska-Lejman, M., Gazecka, M., Henderson, I.R., Higgins, J.D. and Ziolkowski, P.A. *MSH2* stimulates interfering and inhibits non-interfering crossovers in response to genetic polymorphism. *Nat Commun*. 2023; 14:6716.
141. Wang, L., Sun, Y., Sun, X., Yu, L., Xue, L., He, Z., Huang, J., Tian, D., Hurst, L.D. and Yang, S. Repeat-induced point mutation in *Neurospora crassa* causes the highest known mutation rate and mutational burden of any cellular life. *Genome Biol*. 2020; 21:142.
142. Selker, E.U. Premeiotic instability of repeated sequences in *Neurospora crassa*. *Annu Rev Genet*. 1990; 24:579-613.
143. Gladyshev, E. Repeat-induced point mutation and other genome defense mechanisms in fungi. *Microbiol Spectr*. 2017; 5:10.1128/microbiolspec.FUNK-0042-2017.
144. Li, W.C., Huang, C.H., Chen, C.L., Chuang, Y.C., Tung, S.Y. and Wang, T.F. *Trichoderma reesei* complete genome sequence, repeat-induced point mutation, and partitioning of CAZyme gene clusters. *Biotechnol Biofuels*. 2017; 10:170.
145. Rose, D., Thomas, W. and Holm, C. Segregation of recombined chromosomes in meiosis I requires DNA topoisomerase II. *Cell*. 1990; 60:1009-1017.
146. Goldstein, A.L. and McCusker, J.H. Three new dominant drug resistance cassettes for gene disruption in *Saccharomyces cerevisiae*. *Yeast*. 1999; 15:1541-1553.
147. Schwacha, A. and Kleckner, N. Identification of joint molecules that form frequently between homologs but rarely between sister chromatids during yeast meiosis. *Cell*. 1994; 76:51-63.

148. Chen, Y.K., Leng, C.H., Olivares, H., Lee, M.H., Chang, Y.C., Kung, W.M., Ti, S.C., Lo, Y.H., Wang, A.H., Chang, C.S. *et al.* Heterodimeric complexes of Hop2 and Mnd1 function with Dmc1 to promote meiotic homolog juxtaposition and strand assimilation. *Proc Natl Acad Sci U S A*. 2004; 101:10572-10577.
149. Hernlem, B. and Hua, S.S. Dual fluorochrome flow cytometric assessment of yeast viability. *Curr Microbiol*. 2010; 61:57-63.
150. Chen, Y.J., Chuang, Y.C., Chuang, C.N., Cheng, Y.H., Chang, C.R., Leng, C.H. and Wang, T.F. *S. cerevisiae* Mre11 recruits conjugated SUMO moieties to facilitate the assembly and function of the Mre11-Rad50-Xrs2 complex. *Nucleic Acids Res*. 2016; 44:2199-2213.
151. Bishop, D.K., Park, D., Xu, L. and Kleckner, N. *DMC1*: a meiosis-specific yeast homolog of *E. coli* recA required for recombination, synaptonemal complex formation, and cell cycle progression. *Cell*. 1992; 69:439-456.
152. Koren, S., Walenz, B.P., Berlin, K., Miller, J.R., Bergman, N.H. and Phillippy, A.M. Canu: scalable and accurate long-read assembly via adaptive k-mer weighting and repeat separation. *Genome Res*. 2017; 27:722-736.
153. Schwacha, A. and Kleckner, N. Interhomolog bias during meiotic recombination: meiotic functions promote a highly differentiated interhomolog-only pathway. *Cell*. 1997; 90:1123-1135.